(4)

Applied Research Laboratory
The Pennsylvania State University

HIGH REYNOLDS NUMBER LIQUID FLOW MEASUREMENTS

by

G. C. Lauchle, M. L. Billet, S. Deutsch

ARL:PSU

TECHNICAL REPORT

(4)

The Pennsylvania State University
APPLIED RESEARCH LABORATORY
P. O. Box 30
State College, PA 16804

HIGH REYNOLDS NUMBER LIQUID FLOW MEASUREMENTS

by

G. C. Lauchle, M. L. Billet, S. Deutsch

N00024-85-C-6041

Technical Report No. TR 88-012

August 1988

Supported by:
ONR, ONT, NAVSEA, SPAWAR

L. R. Hettche, Director
Applied Research Laboratory

Approved for public release; distribution unlimited

Unclassified
SECURITY CLASSIFICATION OF THIS PAGE

REPORT DOCUMENTATION PAGE

1a REPORT SECURITY CLASSIFICATION Unclassified	1b RESTRICTIVE MARKINGS
2a SECURITY CLASSIFICATION AUTHORITY	3 DISTRIBUTION / AVAILABILITY OF REPORT Unlimited
2b DECLASSIFICATION / DOWNGRADING SCHEDULE	
4 PERFORMING ORGANIZATION REPORT NUMBER(S)	5 MONITORING ORGANIZATION REPORT NUMBER(S)
6a NAME OF PERFORMING ORGANIZATION Applied Research Laboratory The Pennsylvania State University 6b OFFICE SYMBOL (If applicable) ARL	7a NAME OF MONITORING ORGANIZATION See other side.
6c ADDRESS (City, State, and ZIP Code) P. O. Box 30 State College, PA 16804	7b ADDRESS (City, State, and ZIP Code) See other side.
8a NAME OF FUNDING / SPONSORING ORGANIZATION 8b OFFICE SYMBOL (If applicable) ONR, ONT, NAVSEA, SPAWAR	9 PROCUREMENT INSTRUMENT IDENTIFICATION NUMBER
8c ADDRESS (City, State, and ZIP Code)	10 SOURCE OF FUNDING NUMBERS PROGRAM ELEMENT NO / PROJECT NO / TASK NO / WORK UNIT ACCESSION NO

11 TITLE (Include Security Classification)
High Reynolds Number Liquid Flow Measurements

12 PERSONAL AUTHOR(S)
Gerald C. Lauchle, Michael L. Billet, Steve Deutsch

13a TYPE OF REPORT	13b TIME COVERED FROM ____ TO ____	14 DATE OF REPORT (Year, Month, Day)	15 PAGE COUNT
		August 1988	69

16 SUPPLEMENTARY NOTATION

17 COSATI CODES			18 SUBJECT TERMS (Continue on reverse if necessary and identify by block number)
FIELD	GROUP	SUB-GROUP	axial flow, fluid flow visualization, hydrodynamics, hydroacoustic variable measurement, measurement technique, multiphase fluid flow, turbomachinery.

19 ABSTRACT (Continue on reverse if necessary and identify by block number)

This report describes state-of-the-art techniques for the measurement of hydrodynamic and hydroacoustic phenomena in high-Reynolds number liquid flows. Emphasis is on water tunnel testing. Topics covered include: facility operations, boundary layers, multiphase flows, body forces and moments, acoustics, and internal flows.

20 DISTRIBUTION / AVAILABILITY OF ABSTRACT ☒ UNCLASSIFIED/UNLIMITED ☐ SAME AS RPT ☐ DTIC USERS	21 ABSTRACT SECURITY CLASSIFICATION Unclassified
22a NAME OF RESPONSIBLE INDIVIDUAL	22b TELEPHONE (Include Area Code) / 22c OFFICE SYMBOL

DD FORM 1473, 84 MAR 83 APR edition may be used until exhausted. All other editions are obsolete.

SECURITY CLASSIFICATION OF THIS PAGE

Unclassified

This report will be published as a chapter in the book: Lecture Notes in Engineering - Advances in Fluid Mechanics Measurements, M. Gad-el-Hak, ed. (Springer-Verlag, Berlin, New York, 1988).

(cont.)
7a. and 7b.

Office of Naval Research
800 North Quincy St.
Arlington, VA 22217

Office of Naval Technology
800 North Quincy St.
Arlington, VA 22217-5000

Naval Sea Systems Command
Washington, DC 20362-5000

Space and Naval Warfare Systems Command
Washington, DC 20363-5100

ABSTRACT

This report describes state-of-the-art techniques for the measurement of hydrodynamic and hydroacoustic phenomena in high-Reynolds number liquid flows. Emphasis is on water tunnel testing. Topics covered include: facility operations, boundary layers, multiphase flows, body forces and moments, acoustics, and internal flows.

This report will be published as a chapter in the book: Lecture Notes in Engineering - Advances in Fluid Mechanics Measurements, M. Gad-el-Hak, ed. (Springer-Verlag, Berlin, New York, 1988).

TABLE OF CONTENTS

TABLE OF CONTENTS (Continued)

HIGH-REYNOLDS NUMBER LIQUID FLOW MEASUREMENTS

Gerald C. Lauchle
Michael L. Billet
Steven Deutsch
Applied Research Laboratory, The Pennsylvania State University, P.O. Box 30, State College, PA 16804

1.0 INTRODUCTION

Liquid flow facilities are usually categorized as towing tanks, seakeeping and maneuvering basins, circulating water channels, blowdown facilities, and water tunnels. A very complete listing of such facilities has been compiled by the 16th International Towing Tank Conference (ITTC) (1985) and it includes most of the major water facilities in the world. A description of new and planned cavitation facilities is given in Holl and Billet (1987). The intent of this chapter is to discuss the various experimental techniques used in hydrodynamic testing at high Reynolds numbers. This usually implies that water tunnels or tow tanks are used. Because Gad-el-Hak (1987) recently reviewed tow tank testing, our emphasis here is on water (or other liquid) tunnel measurements.

Although, in principle, a water tunnel is just a wind tunnel filled with water, there are many substantive differences in their operation that result from the differences in the properties of water and of air. Water, for example, is about 800 times as dense as air. Since the stresses associated with inertia are a function of fluid density, stresses in water (and, in particular, turbulent stresses) and any vibration they cause, will be larger by a factor of about eight hundred. Thus, to measure the statistical characteristics of turbulent fluctuating pressure fields, for example, a water flow will result in a significantly better signal level from the transducer than would be the case in air.

At the same time, the kinematic viscosity of water is lower than that of air by a factor of about 15; hence, a water tunnel is an ideal facility in which to carry out high-Reynolds-number experiments. From the point of view of fluctuating-stress measurements, even at the same Reynolds numbers, the stresses will be some 3-1/2 times larger in water than in air.

Because the speed of sound is about four and a half times greater in water than in air, the Mach number at a given velocity is 0.22 times that in air; hence, compressibility effects are much smaller. At the same Reynolds number, the Mach number will be 68 times smaller in water than in air; hence, radiation of sound to the farfield from turbulence-produced noise is substantially reduced (since this radiation depends on a high power of the Mach number).

Regarding structural excitation, the impedance match between water and most structural materials (being dependent upon the product of density and the speed of sound) is far better than that between air and most structural materials. At either the same Reynolds number or at the same stress levels, the velocities of the flows in

air and water are far different; therefore, the modes excited in the structure will be quite different. Thus, the entire problem of hydroelastic interaction is quite different in water-tunnel operations.

In water the Prandtl number is nearly an order of magnitude higher than it is in air. This means that in water, the transport of heat by molecular motion is about an order of magnitude less effective than the transport of momentum; in air they are comparable. This makes some types of flow visualization, such as Schlieren and holographic photography, and dye injection much more effective in water tunnel testing than in wind tunnel testing.

1.1 Typical Water Tunnels

The Applied Research Laboratory at Penn State University (ARL Penn State) supports and maintains the operation of four (4) water tunnels and a glycerine tunnel. These tunnels are used for both basic and applied research. The Garfield Thomas, 1.22 m diameter Water Tunnel is the largest at ARL Penn State and is also recognized as the largest high-speed water tunnel in the free world. Its basic design and operation are discussed by Lehman (1959). The test section of the 1.22 m tunnel is 4.27 m long and supports water velocities of up to 18.3 m/s. Figure 1 summarizes other physical features of this water tunnel. The next largest water tunnel at ARL Penn State is schematically described in Fig. 2. Its circular test section is 0.30 m diam. X 0.76 m long. Also in use is a rectangular section 0.51 m X 0.11 m X 0.76 m long. Speeds of 24.4 m/s are achieved in the 0.3 m water tunnel. Figure 3 shows a schematic of the 0.15 m water tunnel. Its test section is 0.61 m long and water speeds of 21.3 m/s are achieved. The fourth water tunnel in use at ARL Penn State is an ultra-high speed cavitation tunnel, Fig. 4. Speeds of 83.8 m/s are achieved in the 3.8 cm diameter test section. The facility is particulary well suited to cavitation damage research (Stinebring, et.al., 1980) although some work on cavitation in liquid freon has also been performed, e.g., Holl, et.al. (1975). Used exclusively for fundamental turbulence research, the Boundary Layer Research Facility (BLRF) supports fully-developed turbulent pipe flow of glycerine. Bakewell and Lumley (1967) designed and fabricated this highly unique glycerine tunnel (Fig. 5) which has a test section 0.30 m in diameter X 7.6 m long with a mean flow velocity of 6.1 m/s. The velocity remains constant and the Reynolds number is varied by altering the viscosity of the glycerine through temperature control.

The use of water or liquid tunnels, such as those described above, in high-Reynolds number hydrodynamics and hydroacoustics research is the subject of this chapter. Five general areas of measurement are described: Body Force Measurements, Boundary Layer Measurements, Multiphase Flow Measurements, Hydroacoustic Measurements and Internal Flow Measurements. In any given typical test program, there may be much overlap among these various measurements, but each has its own unique set of procedures. Those techniques, illustrated by examples, are presented here. The chapter represents an extension of two previously published articles on water tunnel

1.22 m WATER TUNNEL (Garfield Thomas)

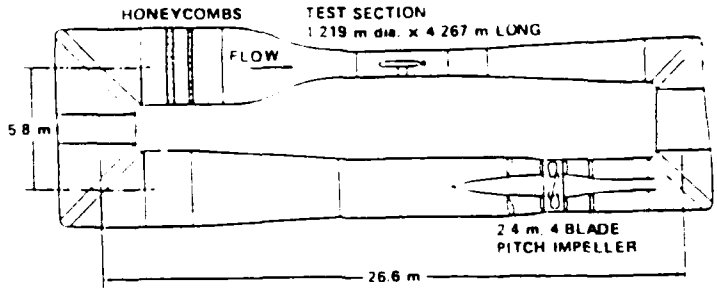

DESCRIPTION OF FACILITY:	Closed Circuit, Closed Jet
TYPE OF DRIVE SYSTEM:	4-Blade Adjustable Pitch Impeller
TOTAL MOTOR POWER:	2000 HP Variable Speed (1491 kw)
WORKING SECTION MAX. VELOCITY:	18.29 m/s
MAX. AND MIN. ABS. PRESSURES:	413.7 to 20.7 kPa

Figure 1. The 1.22 m Diameter Garfield Thomas Water Tunnel

30.5 cm WATER TUNNEL

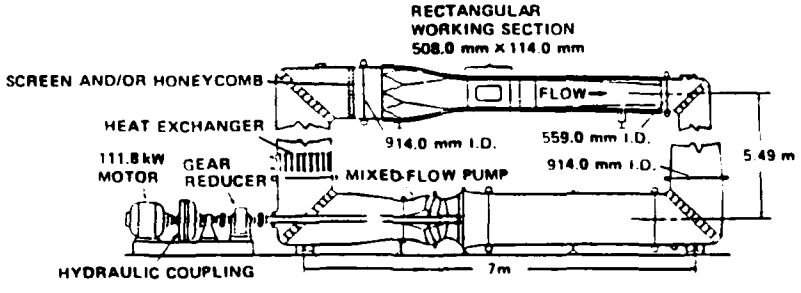

DESCRIPTION OF FACILITY:	Closed Circuit, Closed Jet
TEST SECTIONS:	1) Circular: 304.8 mm dia. × 762.0 mm long
	2) Rectangular: 508.0 mm × 114.3 mm × 762.0 mm
TYPE OF DRIVE SYSTEM:	Mixed Flow Peerless Pump
TOTAL MOTOR POWER:	150 HP (111.8 kw)
WORKING SECTION MAX. VELOCITY:	24.38 m/s
MAX. AND MIN. ABS. PRESSURES:	413.7 to 20.7 kPa

Figure 2. The 30.5 cm ARL Penn State Water Tunnel

15.2 cm WATER TUNNEL

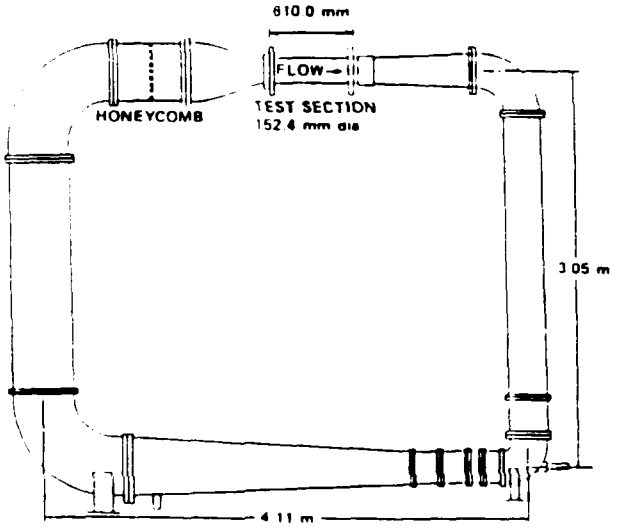

DESCRIPTION OF FACILITY:	Closed Circuit, Closed Jet
TYPE OF DRIVE SYSTEM:	Axial-Flow Pump
TOTAL MOTOR POWER:	25 HP (18.64 kw)
WORKING SECTION MAX. VELOCITY:	21.34 m/s
MAX. AND MIN. ABS. PRESSURES:	861.9 to 20.7 kPa

Figure 3. The 15.2 cm ARL Penn State Water Tunnel

ULTRA-HIGH SPEED WATER TUNNEL

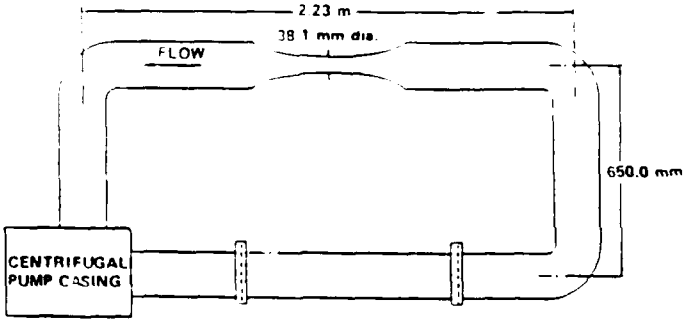

DESCRIPTION OF FACILITY:	Closed Circuit, Closed Jet
TYPE OF DRIVE SYSTEM:	Centrifugal Variable Speed Drive
TOTAL MOTOR POWER:	75 HP (55.9 kw)
WORKING SECTION MAX. VELOCITY:	83.8 m/s
MAX. AND MIN. ABS. PRESSURES:	8274.0 to 41.4 kPa

Figure 4. The 3.8 cm ARL Penn State Ultra-High Speed Water Tunnel

BOUNDARY LAYER RESEARCH TUNNEL (GLYCERINE)

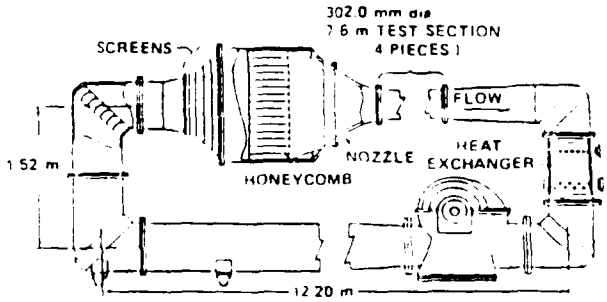

DESCRIPTION OF FACILITY:	Constant Dia. Test Section, Closed Circuit
TYPE OF DRIVE SYSTEM:	Gould Centrifugal Pump
TOTAL MOTOR POWER:	100 HP (74.6 kw)
WORKING SECTION MAX. VELOCITY:	7.62 m/s
MAX. AND MIN. ABS. PRESSURES:	586.0 to 101.4 kPa
TEMPERATURE RANGE:	35°C to 46°C
REYNOLDS NUMBER RANGE:	10,000 - 26,500

Figure 5. The 30 cm ARL Penn State Glycerine Tunnel

testing by Henderson and Parkin (1982) and Parkin (1983). As a preface to specific types of measurement, a brief description of typical water tunnel operation is presented.

2.0 WATER TUNNEL OPERATION

The closed-circuit water tunnel is usually composed of a series of interconnected cylindrical shells of varying cross section. The test section, or working section, is usually a true cylinder. The settling section and nozzle are upstream of the test section and is where turbulence management apparatus is located. Downstream of the test section the flow velocity is slowly decreased by a diffuser section. In order to complete the closed circuit loop, turns are required. These turns must be designed with turning vanes to minimize losses. The pump is located in the lowest leg of the tunnel where the hydrostatic pressures are highest to help suppress pump cavitation. Also the cross sectional areas are largest in this leg so that the flow velocity is minimized.

The two fundamental variables in the test section are velocity and pressure. A well-designed tunnel provides for accurate control of these variables over a wide range. Speed control in the 1.22 m diameter water tunnel at ARL Penn State is achieved by varying the pump impeller rotational speed and the pitch of the impeller blades. This pump is driven by a 2000 HP variable-speed (0-180 rpm) induction motor.

The pitch can be varied over 28 deg. by means of a hydraulic servomechanism which is operated remotely from the tunnel operating console.

The static pressure in the test section must be maintained at a pre-determined value regardless of velocity. Using as an example the 1.22 m water tunnel, this pressure control is achieved by varying the air pressure on the top of a large pressure-regulating tank connected to the bottom leg of the tunnel. This tank (approximately 1 m in diameter X 4 m high) has in it a redwood float that prevents the air from coming in contact with a large surface area of water; a necessary feature when concerned with gas content effects in some hydrodynamics work.

A schematic of the pressure regulating control system is shown in Fig. 6. The air pressure in the pressure-regulating tank, and thus the tunnel pressure, is controlled by a differential pressure transmitter (23), which is supplied with two pressures, one from the working section and the other from the pressure-regulating valve on the console (22). The output from the transmitter is an air pressure whose value indicates whether the working-section pressure is equal to or deviates from the desired pressure. The output is delivered to a controller (25), which will adjust the working-section pressure if a difference exists. The adjustment is achieved by supplying an operating pressure to control valves (15) and (16), which connect the low-pressure-regulating tank with the low- or intermediate-pressure receivers. If, for example, the working-section pressure is low, the valve (15) to the low-pressure receiver, which in normal operation is slightly open, will close and so stop the flow

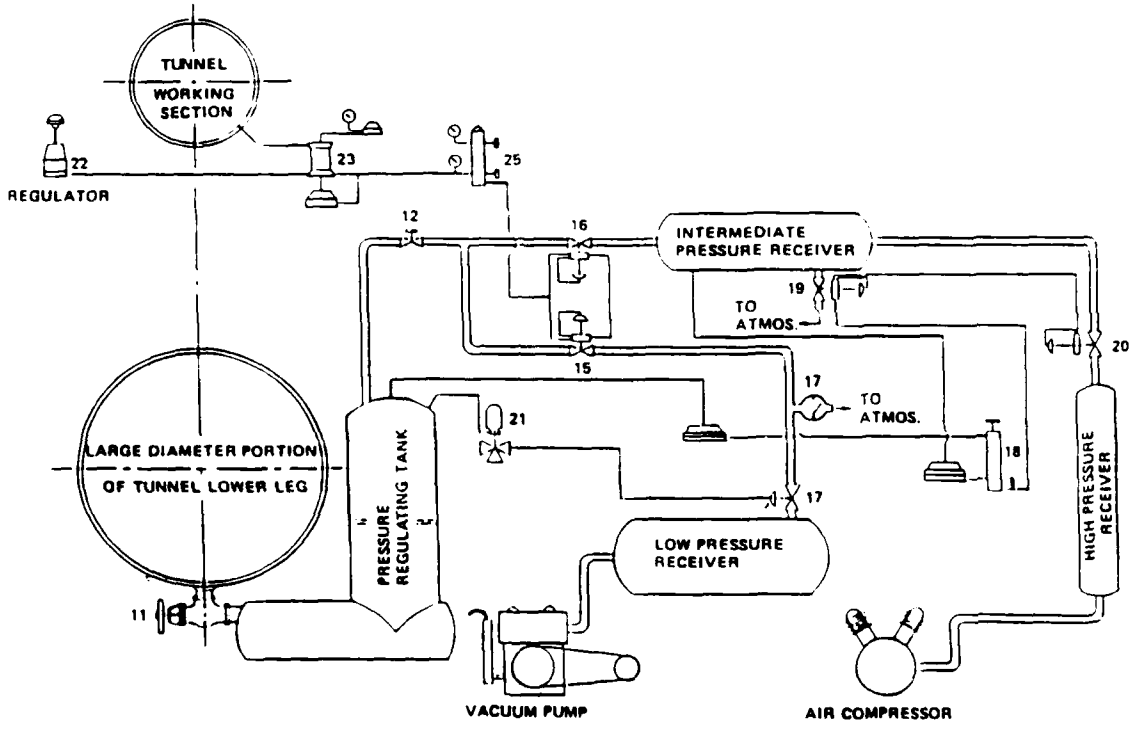

Figure 6. Control System for Tunnel Pressure Regulation (from Lehman, 1959)

from the regulating tank to the low-pressure receiver. At the same time, the valve (16) - which also normally operates while slightly open - will be opened wider so as to permit a greater flow from the intermediate-pressure receivers to the pressure-regulating tank. This situation will continue until the transmitter senses that the tunnel has reached the desired pressure and causes the controller to restore the control valves to their neutral positions. In addition to the control of pressure and velocity, there are other variables that must be considered in specific types of testing. The more important of these are now discussed.

2.1 Water-Conditioning

A water-conditioning system, or bypass system, is shown for the 1.22 m Water Tunnel in Fig. 7. It is used to filter the water, degas the water and if required change the temperature of the water. Because the flow through such a system may be significant (typically 65 l/s), the automatic pressure control system is tied into the bypass circuit (11). With the water level in the pressure-regulating tank equal to the set value, the throttle valve (39) will be adjusted to maintain the flow from the tunnel exactly equal to the flow to the tunnel, that is, from the degasser through the adjustable speed pump to the water tunnel. As the water level deviates from the set value, the throttle valve will open or close as required, increasing or decreasing the flow from the tunnel to the degasser so as to restore normal conditions.

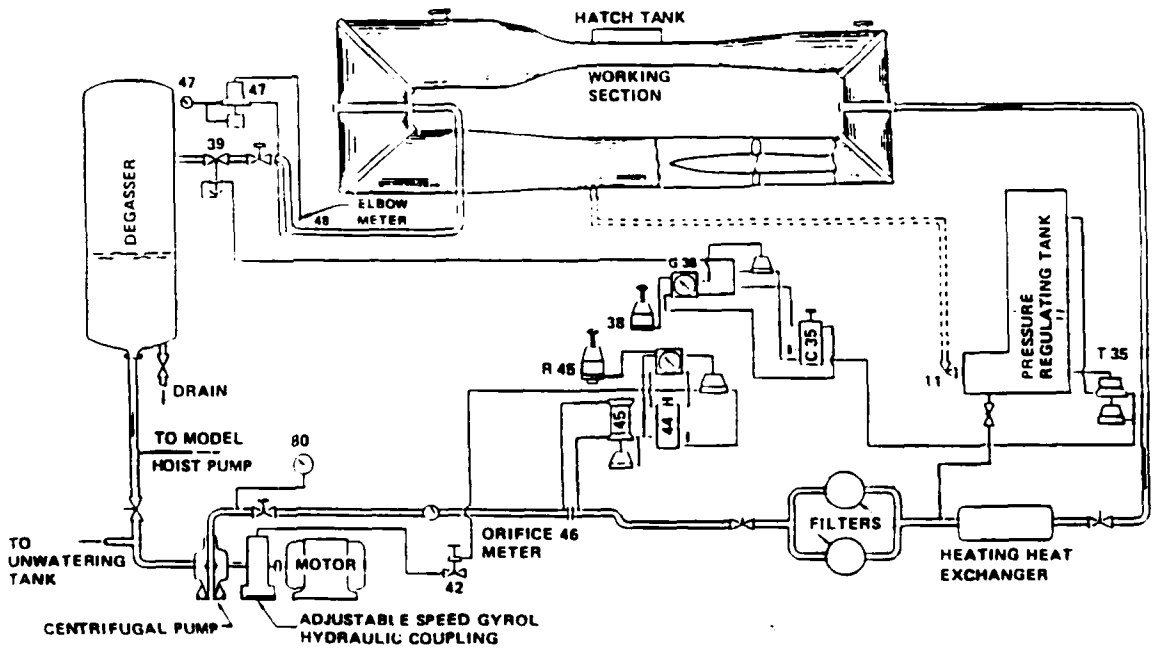

Figure 7. Tunnel Bypass System (from Lehman, 1959)

All water that enters the tunnel from the main lines or well must enter through the bypass system, in which there are two filters of 10 μm porosity. With the bypass system operating, tunnel water is continually filtered. Of particular importance in

cavitation research and in some types of drag reduction research is the air content level of the water. Gas removal from the water is accomplished with a Cochrane Cold-Water Degasifier located in the bypass circuit. The degasser consists of an upright cylindrical tank approximately 2 m in diameter and 6 m high. The upper portion of this tank is filled with plastic saddles which are approximately 3.8 cm high and 7.6 cm in outside diameter. Water taken from the tunnel through the bypass system is sprayed into the top of the tank, the interior of the tank being maintained at a high vacuum of approximately 71 cm of mercury. The water spray falling over the saddles distributes the water in thin films, and exposure of these films to the vacuum permits the rapid removal of dissolved air. The water collects in the bottom of the degasser and returns to the bypass system.

Operation of the degasser permits the lowering of the gas content in the tunnel from about 15 parts per million by molecular weight to around two or three parts per million in approximately three hours. On occasions when an increase in the gas content is desired, one of two methods are utilized. Small increases in gas content are achieved by using the Cochrane Cold-Water Degasifier located in the bypass circuit with the tank pressurized. When levels near saturation are required, fresh water is added to the tunnel circuit. Air is not normally added to the tunnel to increase the air content level because often times large bubbles persist.

The Reynolds number of a given flow in a water tunnel can be varied by changing either the tunnel velocity or the water temperature (or both). The 1.22 *m* tunnel provides (as part of the bypass system) for water heating. The useful temperature range of 10 to 49 deg. C permits the Reynolds number to be changed by a factor of two (2). This capability has proved useful when measuring drag coefficients on small bodies. The small bodies are necessary to minimize spurious measurement errors due to wall effects, but by operating at high temperatures, the Reynolds number range of a larger body is preserved. Higher than normal water temperatures have also been used in transition research where the demonstration of high transition Reynolds numbers by wall heating or suction was the goal. The higher water temperature effectively raises the unit Reynolds number range of the facility.

2.2 Turbulence Control

Low freestream turbulence levels in the working section of a water tunnel are absolutely necessary for many studies in hydrodynamics. This is particularly true when studying high-Reynolds number laminar flows and the transition process. Although screens have been used to reduce turbulence in wind tunnels, they are not particulary satisfactory in water tunnels; that is, large, high-speed water tunnels. The problem with screens is strength. The wire diameter required for a given velocity of operation almost always results in a wire diameter Reynolds number range where vortex shedding occurs. This shedding causes the familiar "singing" phenomenon.

Based on the fundamental work of Lumley (1964) and Lumley and McMahon (1967), honeycombs in which the cells have a large length-to-diameter ratio have been used

successfully to reduce turbulence levels to order 0.1% in the ARL Penn State tunnels. The honeycomb has two effects: it reduces the level of existing turbulence, and it creates turbulence of its own. With the right design of honeycomb, the combined effect is favorable. The honeycomb completely annihilates the transverse components (u_2 and u_3) of velocity, and so only the u_1 component remains immediately downstream of the honeycomb. However, the turbulence has a very strong tendency to rearrange itself and return to an isotropic state. This state is influenced to a significant degree by the flow within individual cells. It is advantageous to have fully-developed turbulent flow in the cells as opposed to laminar or transitional flow. This surprising conclusion (Lumley and McMahon, 1967) is based on the fact that a laminar wake exiting the honeycomb cell is actually larger than a turbulent wake and it produces more turbulence than is lost in the laminarization of the cell flow. It is therefore accepted procedure to leave rough edges on honeycomb that has been sawed to size. This roughness lowers the cell transition Reynolds number.

Placement of turbulence management honeycomb in the plenum section just upstream of the nozzle section has advantages. The turbulence at the exit of the honeycomb enters the nozzle contraction and eddies are stretched (elongated) axially. This upsets the isotropic state again and the fluctuating transverse velocities are reduced. The degree of turbulence suppression by the nozzle depends on the contraction ratio. Ramjee and Hussain (1976) report on these effects of contraction ratio, and show that the larger the contraction, the greater the turbulence suppression.

For example, the 1.22 m Water Tunnel uses honeycomb with hexagonal cells 47.6 cm long X 0.56 cm across the flats. This is placed 1.39 m upstream of the nozzle which has a 9:1 contraction ratio. Robbins (1978) measured the turbulence levels and length scales in both the plenum and test section before and after installation of the honeycomb. Figure 8 shows the axial component of turbulence intensity in the test section. The level of 0.1% for velocities greater than 10 m/s is quite acceptable for most work. The high turbulence levels at lower velocities are a result of transitional flow in the honeycomb and support the Lumley and McMahon recommendation noted above. The open circles of Fig. 8 represent plenum data extrapolated to the test section using theory developed by Lumley and McMahon (1967).

A high-Reynolds number laminar pipe flow facility is described by Barker and Gile (1981). They used a honeycomb and screens upstream of a 35:1 contraction ratio nozzle to achieve test section turbulence levels of order 0.01% which is better than most wind tunnels. It demonstrates that turbulence levels in water tunnels can be made extremely low provided one can justify the large contraction ratio nozzle and entrance flow control. With very large contraction ratios, the boundary layer separates at the test section entrance which then feeds new turbulence into the working volume. Barker and Gile needed to provide wall suction in this critical region to control the separation.

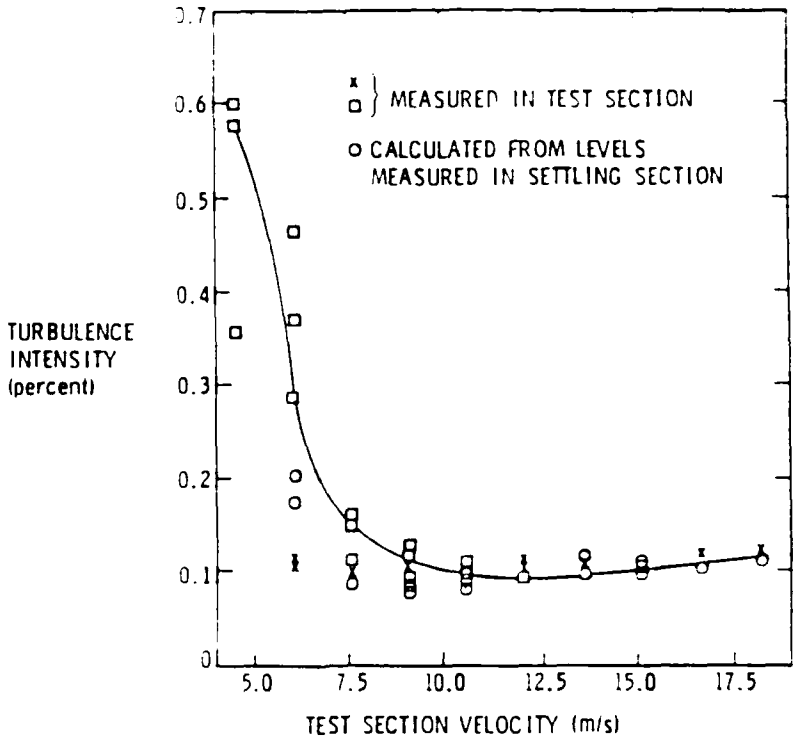

Figure 8. Turbulence Intensity (axial component) in 1.22 m Diameter Water Tunnel Test Section

2.3 Noise Control

Unfortunately, the control of background noise in a water tunnel is at least an order of magnitude more difficult than the control of turbulence, water quality, pressure, or velocity. The reason is hydroelastic in nature. The metallic materials used in water tunnel construction have a density comparable to that of water. Conventional methods of noise path attenuation become severely limited because there are two paths of transmission: one through the water and the other through the structure. One can place an acoustic baffle in the liquid that attenuates the water-borne path, but the energy on the source side of the baffle "jumps" into the structure at that point, bypasses the baffle, and then re-enters the water and continues to propagate through the water. The same thing happens if one baffles the structure, say with a rubber gasket at a joint. Structure-borne energy leaves the structure at the gasket, travels through the water, and then back into the structure. Thus the only way to attenuate the duct modes of acoustic energy flow is by blocking both water and structure paths simultaneously and at the same point. Attempts at doing this by many organizations to existing facilities have been generally unsuccessful. However, several planned facilities have attempted to incorporate these ideas in their design (Holl and Billet, 1987).

Water tunnels that are relatively quiet, have relatively quiet sources of noise. The primary source is the pump. Secondary sources are separation zones in turns and

wall turbulent boundary layers. A typical tunnel can be quieted by 15 to 30 dB through complete suppression of pump cavitation. The CALTECH High-Speed Water Tunnel (Barker, 1974), the NUSC, New London Acoustic Water Tunnel (Schloemer, 1974), and the ARL Penn State 1.22 m Water Tunnel (Lauchle, 1977) are all capable of operating cavitation free; thus, they are fairly quiet tunnels. The NUSC, New London tunnel also uses fire hose in parts of the circuit to help suppress vibration.

Even with a quiet pump and well-designed turns, the turbulent boundary layer in the test section and diffuser radiate significant acoustic energy. Typical spectral data for this clear tunnel noise are shown for the CALTECH and ARL Penn State tunnels in Fig's. 9 and 10, respectively. Even though the 1.22 m tunnel is larger than the CALTECH tunnel by a factor of about four (4), it is quieter. The reason is due to the physics of turbulent boundary layer (TBL) noise, e.g. Tam (1975). The noise spectrum peaks when $\omega\delta^*/u=8\times10^{-2}$ (ω = radian frequency, δ^*=TBL displacement thickness, u=velocity). The smaller water tunnel supports a thinner TBL at the end of the test section than does the larger tunnel at the same velocity. Consequently, the peak in TBL noise occurs at a higher frequency; the roll-off portion of the TBL noise spectrum is at a higher level and is within the frequency range shown on Fig's. 9 and 10. At ultra-low frequencies, the larger water tunnel would be the noisier of the two.

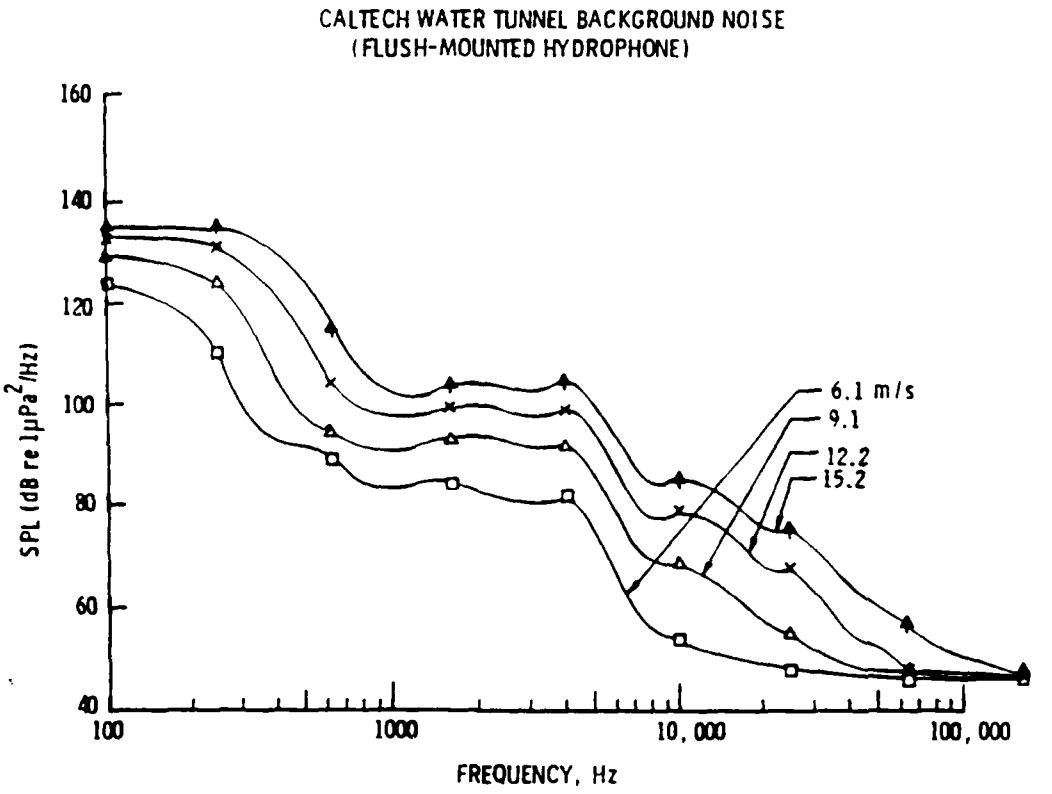

Figure 9. Clear Tunnel Background Noise of CALTECH Water Tunnel

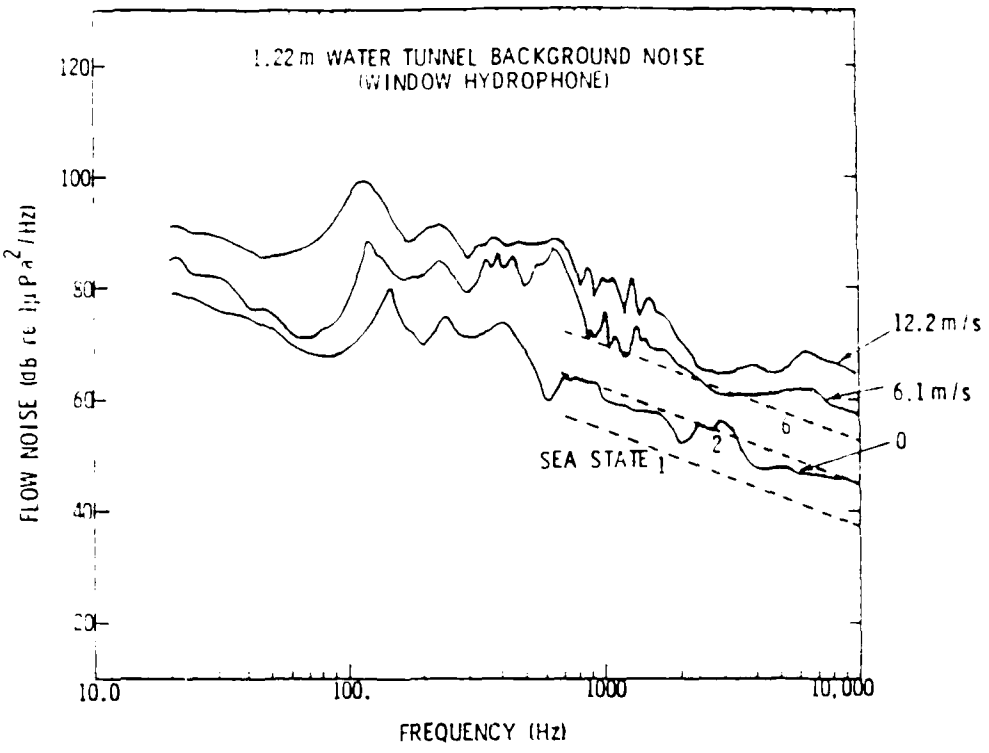

Figure 10. Clear Tunnel Background Noise of ARL Penn State 1.22 m Water Tunnel

3.0 BODY FORCE MEASUREMENT

Although the standard facility used to determine body forces and moments, and powering (or propulsion) characteristics of marine-type vehicles is the towing tank, these facilities are limited to relatively low velocities (5-8 m/s) for completely submerged bodies. This limitation is caused by surface wave effects and the water-piercing strut interference drag. The Reynolds number range is often low and accurate scaling of the powering or force data to larger prototype conditions is difficult.

The water tunnel is most useful for the testing of completely submerged bodies. Higher Reynolds numbers can be achieved so that the scaling of data is more accurate. If the body frontal area is greater than about 1/40 the test section cross sectional area, then complications may arise from tunnel wall interference effects, e.g. Ross, et.al. (1948). The tunnel wall causes the streamlines over the body to be modified which changes the body pressure distribution from that observed in a free-field environment. In addition, the skin friction and displacement thickness growth over the body and tunnel wall give rise to a spurious axial force component called horizontal buoyancy. Much of the potential flow blockage effect and part of the horizontal buoyancy effect can be eliminated by using a flow correcting liner attached to the test section wall, Fig. 11. The fundamental research on liner design was performed by Lehman, et.al. (1958) and Peirce (1964). The basic premise in liner design is that if the tunnel wall were to conform exactly to one of the outer stream

surfaces formed when the body operates in the free stream, then all forces acting on the body would be unaffected by the tunnel wall. The design accuracy therefore depends upon the accuracy that one can predict the stream surfaces over arbitrary bodies. As computational tools and techniques improve, so do tunnel liner designs.

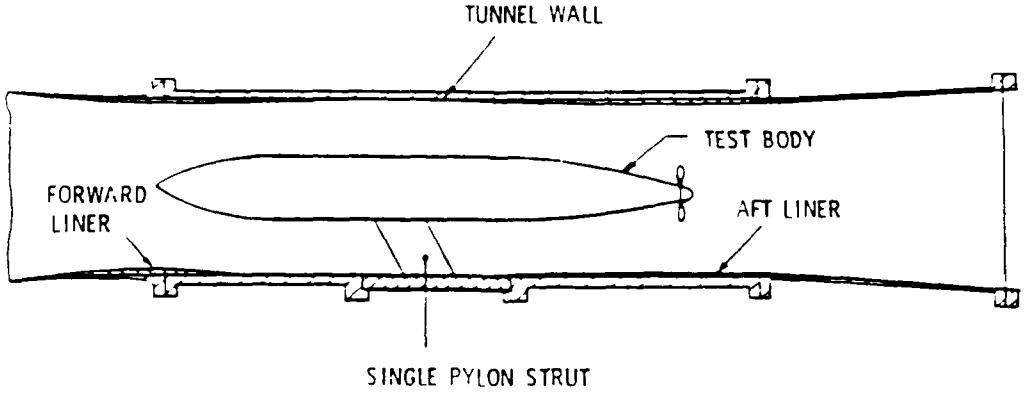

Figure 11. Installation of a Large Body in Water Tunnel Test Section

The liner design resulting from potential flow calculations can (and should) be modified to account for the boundary layer displacement thickness growth over the liner itself. Axisymmetric viscous flow codes can be used for this. The displacement thickness calculated is added to the coordinates of the liner specified in the potential flow calculation. This step accounts for some of the horizontal buoyancy effect, but not all of it. The skin friction on both the body and tunnel wall add to the tunnel interference and cannot be treated easily in the liner design. It is usually handled empirically.

As an example of the empirical procedure, consider the measurement of net axial force on a large axisymmetric body operating in a cylindrical test section with liner. (The force sensors are described in Section 3.1). This body is large enough that tunnel interference effects are present. The body is presumed to have an operating propulsor. A standard propulsor powering test entails measuring the net body axial force, C_X, as a function of the propulsor advance ratio, e.g., Fig. 12 (a). At the self propulsion point, $C_X = 0$. However, C_X = (Thrust) minus (Bare Body Drag) (and bare body drag is affected by tunnel interference) so the true self propulsion point cannot be determined from the data measured. One must remove the propulsor and measure the bare body drag coefficient as a function of Reynolds number, Fig. 12(b). These data must then be compared to the drag coefficient data measured on a very small body of the same geometry. Usually, the Reynolds number range can be maintained between the two tests by operating the small body at much higher speeds and by heating the tunnel water. The difference between the two data sets is the empirical tunnel correction. It is applied, as shown in Fig. 12(a), to the powering data. The primary reasons why the entire test is not conducted at the very-small body scale is that propulsors cannot be manufactured accurately at those scales. Also, the small

electric motors needed to drive the propeller shaft do not supply sufficient power to cover the advance ratio and Reynolds number range of interest. Additional details on this procedure are given by Hall (1973).

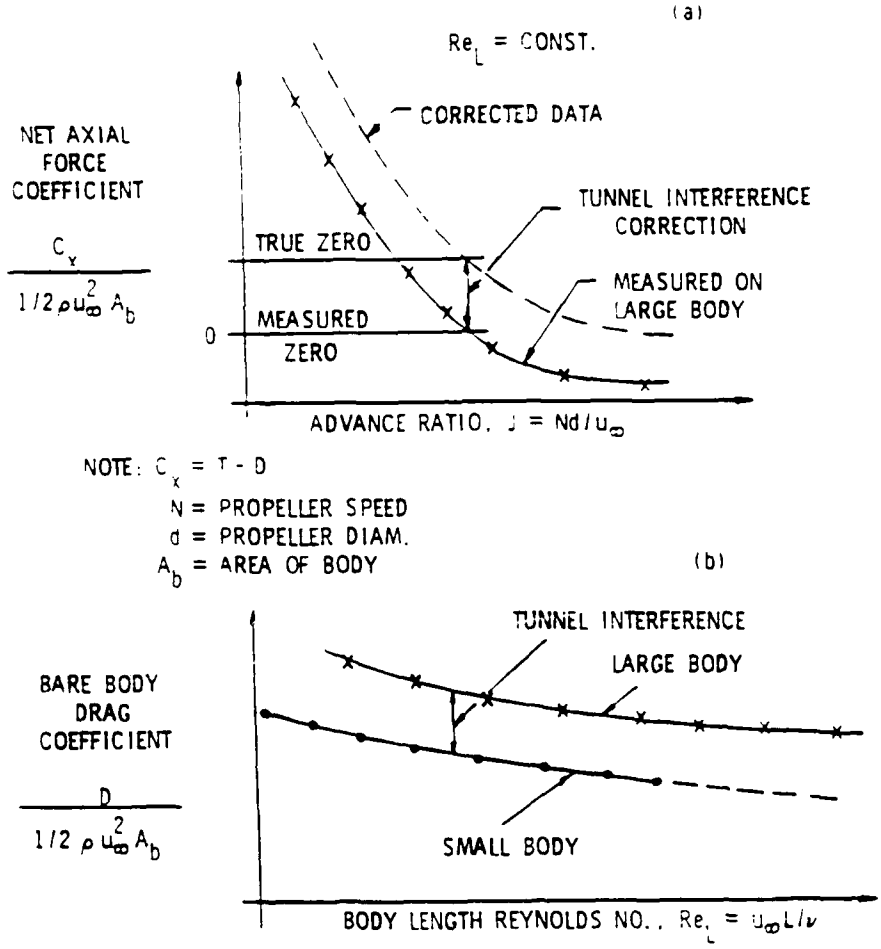

Figure 12. Tunnel Interference Correction Scheme; (a) Net Axial Force Coefficient for Body with Propeller; (b) Bare Body Drag Characteristics

Tunnel wall and horizontal buoyancy effects have a strong influence on the body static pressure distribution. Figure 13, for example, shows a predicted potential flow pressure distribution (which accounts for solid blockage effects) over a large streamlined body whose maximum diameter is 26% of the tunnel diameter (r_w = tunnel wall radius). Also shown on this figure are data obtained at various Reynolds numbers. The discrepancy between data and theory is the horizontal buoyancy effect which is viscous in origin. Lauchle (1979, 1983) has analyzed this problem and derives a closed-form solution for its correction. Figure 14 shows a result of the correction procedure applied to the potential flow solution. The agreement with data is good. One could use this approach, which entails calculating the boundary layer and shear stress distributions over the body and tunnel wall, to estimate accurate

pressure distributions. Accurate pressure distributions are required when studying laminar boundary layer stability and transition, e.g. Lauchle, et.al. (1980).

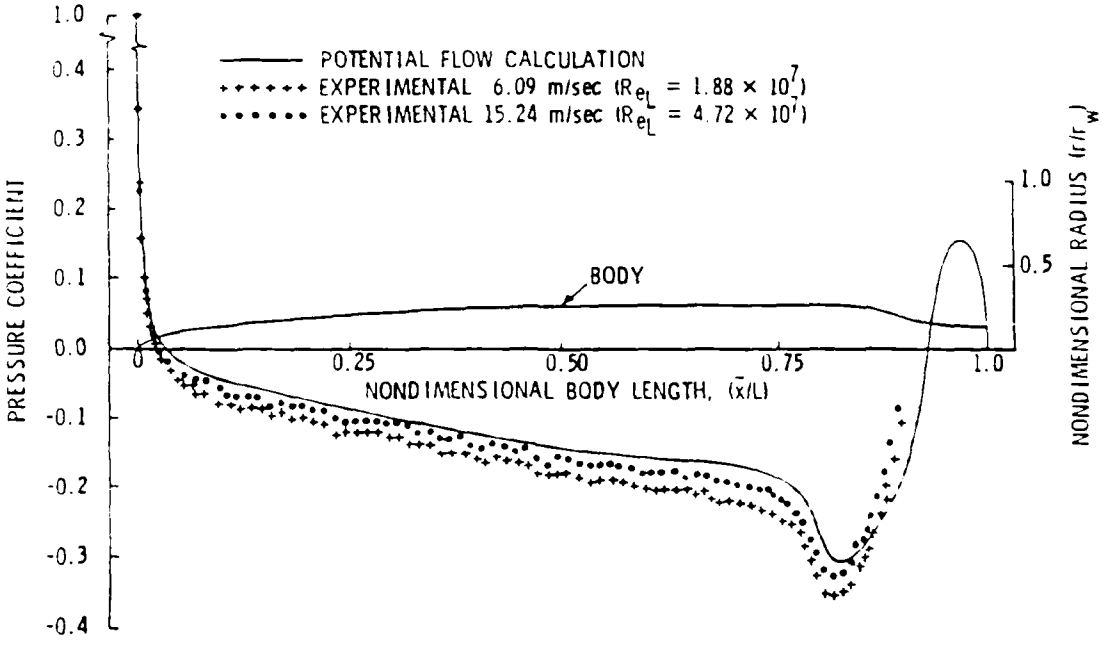

Figure 13. Measured and Predicted Body Pressure Distribution for a Large Body in the 1.22 m Water Tunnel

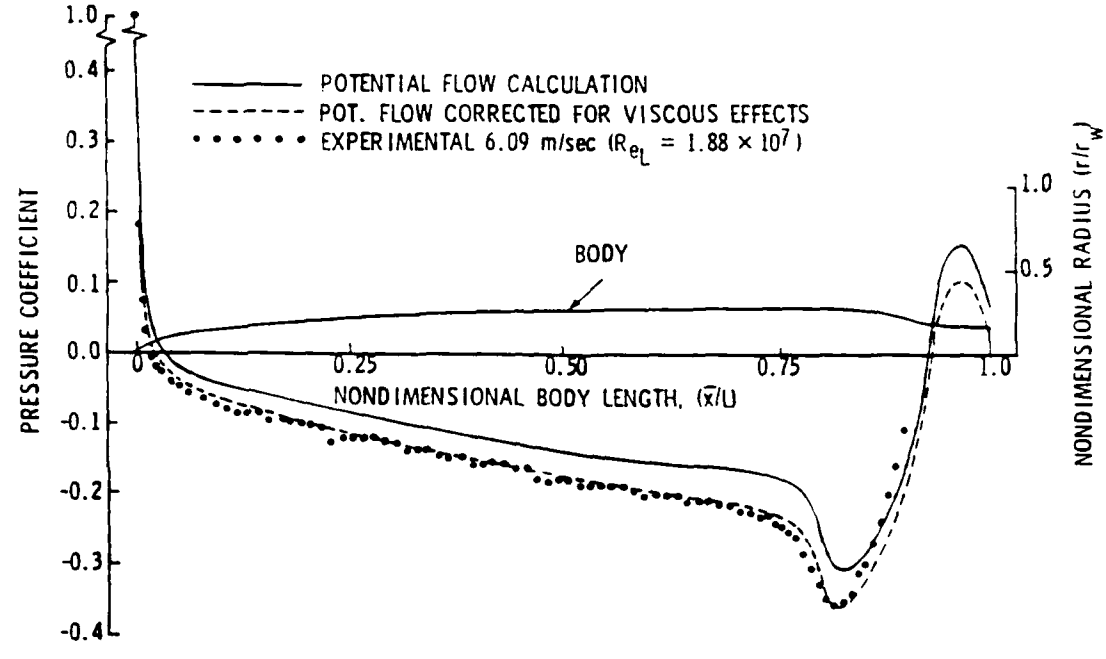

Figure 14. Corrected In-Tunnel Pressure Distributions Accounting for Horizontal Buoyancy Effects

3.1 Force Sensors

Measuring body forces and moments on water tunnel test bodies requires devices that are stiff and insensitive to changes in tunnel pressure. These devices are called balances. The basic element in balance design is the tension member, torque tube, or shear beam. Each balance is designed to meet the objective of the given test program.

A typical force cube with a tension member (Fig. 15) is instrumented with strain gages. The very small elongation of the member, caused by the hydrodynamic force being measured, is sensed directly by the gages. The force and strain are parallel to each other which minimizes cross coupling with other forces. The thin webs that connect the upper tension member side to the base (or ground) side of the cube are called flexure members; they act as double cantilever beams. Notice that the device is extremely rigid in the vertical plane while weak in the horizontal plane. However, the pre-tensioned tension members restore rigidity to the horizontal motion. In operation, the center of the tension member remains fixed to a rigid portion of the model strut system, while the ends are fastened to the body skin subject to the hydrodynamic load of concern. The load causes a microscopic translation of the cube in the left/right direction. One side of the tension member elongates while the other relaxes. The four-arm bridge becomes unbalanced and a voltage is created in the wheatstone bridge circuit that is proportional to load.

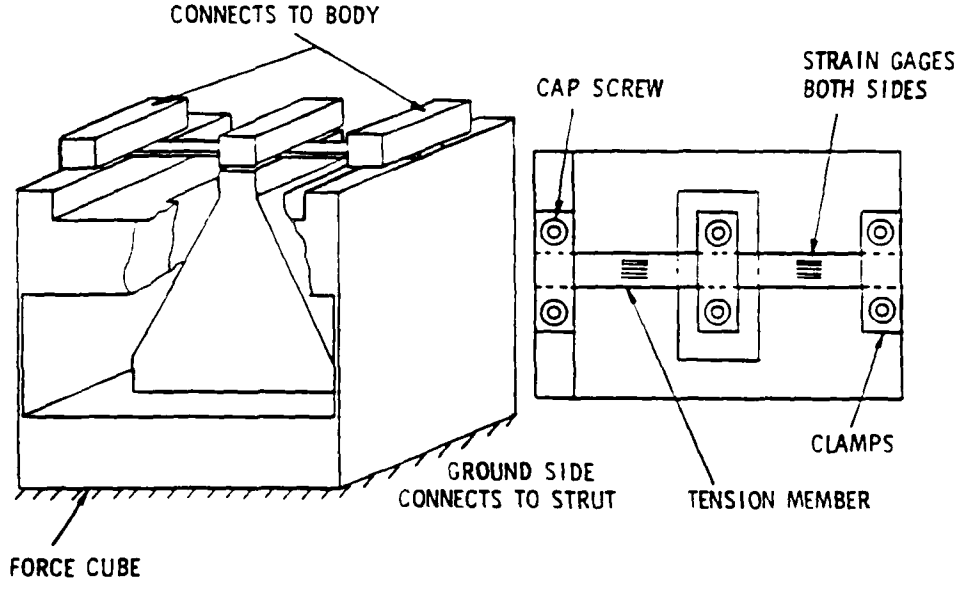

Figure 15. Force Cube - Tension Member Design Concept

Shear beam balances are schematically shown in Fig. 16. In these devices, a web replaces the tension member and the applied force causes shear in the web. The strain gages are placed in a 45° direction to the force so that the principal stress is sensed. The modified shear balance has a reduced area web to increase the shear stress which improves sensitivity further.

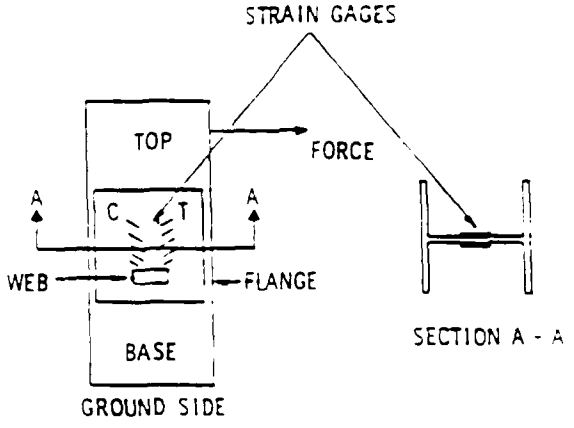

SHEAR BEAM BALANCE

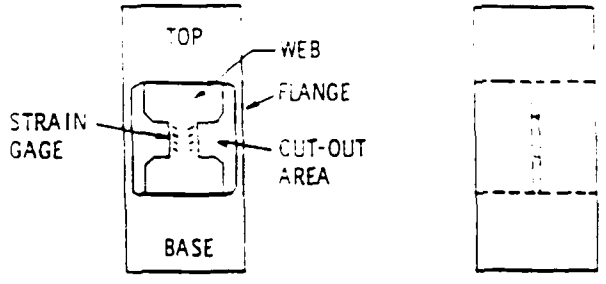

MODIFIED SHEAR BEAM BALANCE

Figure 16. Shear Beam Balance Design Concepts

A torque tube (or cell) is used to measure moments about its longitudinal axis. This includes hinge moments on control surfaces and torque on propulsor shafts. The typical torque cell is shown in Fig. 17. In rotating systems, slip rings are required to bring the strain gage signals out of the test apparatus.

In any given test program, the test body may employ several steady-state force sensors simultaneously. Figure 18 shows a typical experimental setup in which body axial force, propulsor shaft torque, thrust, and control surface hinge moment are all measured.

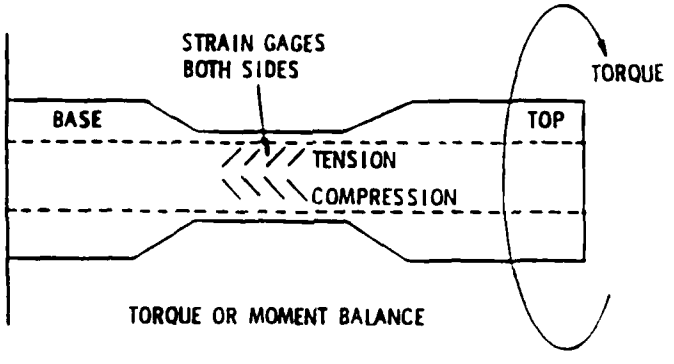

Figure 17. Torque or Moment Balance Design Concept

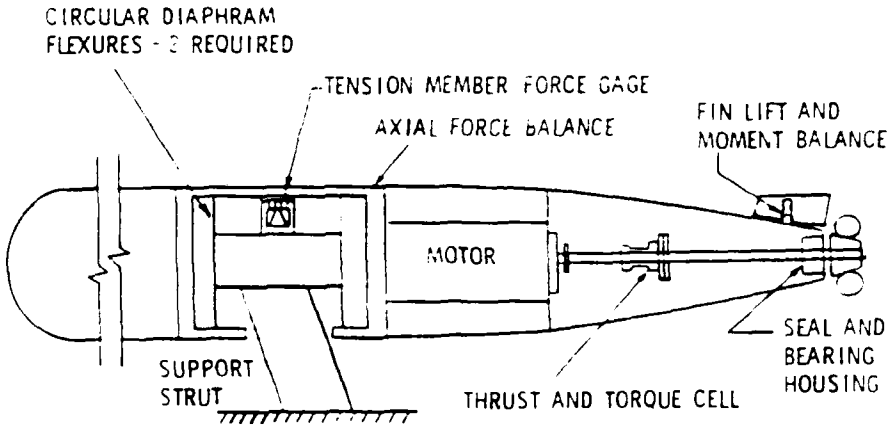

Figure 18. Typical Application of Force and Moment Balance in Water Tunnel Model

The frequency response of strain-gaged force balances is generally poor compared to other dynamic sensors. However, for frequencies less than about 250 Hz, they can provide reliable time-dependent force data. Figure 19 shows an example of this. A large, electrically-heated body (Lauchle and Gurney, 1984) was equipped with a drag force balance in the sting mount. The body could be made to have intermittent laminar flow by adjusting the heating level (heat stabilizes laminar layers in water) to a critical level for the velocity of flow considered. Turbulent spots were created randomly over the body surface and these cause time-random changes in skin friction. A hot film senses the spots where a conditioned hot film output is shown as I(t) on Fig. 19. Here, I(t) is equal to one when a spot is present. The simultaneous drag signal is also shown. The data show clearly the correlation between the presence of turbulent spots in a laminar boundary layer and the instantaneous increases in body drag. Some spikes in drag are not correlated with the indicator function because some spots occur on the opposite side of the body from where the hot film is located.

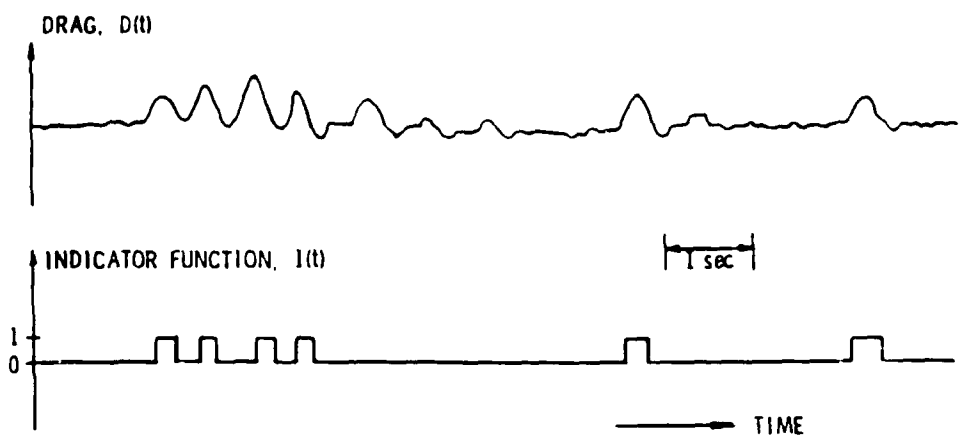

Figure 19. Time Dependent Drag Data Compared with Occurrence of Turbulent Spots on a Laminar Flow Body

Sensors designed specifically for unsteady force measurements usually use a piezoelectric crystal rather than strain gages. This is due primarily to resonance problems with strain gage beams. An application of this technique to the measurement of time-dependent propeller shaft forces is given by Thompson (1976). Non-steady lift measurement techniques are reviewed by Sevik (1964), and Lauchle (1974) presents a technique for measuring unsteady hinge moments.

4.0 BOUNDARY LAYER MEASUREMENTS

4.1 Turbulent Boundary Layers

Turbulent boundary layer measurements in high-speed water tunnels are in general made difficult by the high dynamic pressures involved, by the conductivity and general uncleanliness of the water, by cavitation and by the very small inner boundary layer scales. Of these potential problems, all but the last can be circumvented (more or less simply) in some way, and moreover, are not problems unique to boundary layer measurements. We shall concentrate, therefore, on the problem of very small inner boundary layer scales, and the constraints that they put on the types of measurements we can make and how we have learned to work within these constraints. As in recent years much of the boundary layer work done at ARL Penn State has been driven by the need to understand the mechanics of turbulent drag reduction--a phenomenon dominated by near wall effects--these constraints have been keenly felt.

Typical values of the momentum thickness Reynolds number, for fully developed turbulent boundary layers, which have been measured in our laboratory range from 3000 to 15000. Using approximate relationships found in White (1974), for example, we find sublayer thicknesses (y^+=5) which vary from 5 microns at 18 m/sec to 40 microns at 3 m/sec. Some measured data are shown in Table 1, which is reprinted from Deutsch and Castano (1986). The friction velocity, u_τ, is found for the data shown in Table 1 by requiring a least square fit of the data to the law of the wall (Coles and Hirst, 1968).

We have been most successful, over the past decade, with techniques that measure at the surface of the flow and with LDV techniques. Surface measurement techniques have included skin friction balances, flush mounted hot film gauges and pressure probes. Pressure probes are discussed further in Section 6.3, so that we shall concentrate here on the other three techniques.

Central to all the skin friction balance measurements that we have made, have been floating elements supported by strain-gauged force members. Early designs used the force member in bending, and although this allowed for excellent sensitivity, motion of the balance with increasing velocity was fairly large, typically on the order of several hundred microns for a speed change of 15 m/sec. This movement of the balance section made installation exceedingly difficult. In addition, it raised questions about the alignment of the balance with speed. Subsequent balance sections used an I-beam force member in shear. It was found that sensitivity could be maintained, while the stiffer balance sections were much easier to align and to maintain aligned. Movement of the shear beam balances is on the order of 2.5 microns

TABLE 1. Comparison of LDV data.

Flat Plate

Location* (mm)	U_∞ (m/sec)	R_θ	u^+ (m/sec)	y at $y^+ = 5$ (μm)
272	4.68	3372	0.195	25.6
	10.90	7358	0.423	11.8
374	4.75	4215	0.190	26.3
	10.30	8862	0.392	12.7
454	4.78	5127	0.188	26.6
	10.47	10627	0.392	12.7

Axisymmetric Body

Location** (mm)	U_∞ (m/sec)	R_θ	u^+ (m/sec)	y at $y^+ = 5$ (μm)
255	5.26	2635	0.21	23.8
	10.71	5062	0.405	12.3
	16.94	8837	0.607	8.24
277	5.25	3491	0.21	23.8
	10.77	6764	0.406	12.3
	16.86	10144	0.617	8.10
403	5.30	3775	0.210	23.8
	10.90	8191	0.413	12.11
	16.88	14197	0.594	8.42

* From Virtual Origin
** From Trip Wire

Typically, we have used balance sections with surface areas of 2.5×10^{-3} m^2 in fully developed turbulent boundary layers. The state of the boundary layer is determined beforehand through LDV measurements. On a skin friction balance of this size the force will vary from 0 to about 10 Newtons over the speed range of 0 to 17 m/s. Some appreciation for the linearity and sensitivity of the balance can be obtained by considering a sample output, which is shown in Fig. 20[1].

Problems with balance measurements are generally caused by pressure gradient effects, balance misalignment and, in water, waterproofing. Waterproofing of the strain gauge section is certainly more art than science and we merely note that with too thick a layer of waterproofing one will trade linearity for hysteresis, while too

thin a coating will lead to electrical shorting and balance failure. Uncertainty in the measured pressure gradient is magnified in the skin friction measurement. For example, a nominally zero, measured, pressure gradient is shown in Fig. 21. If the variation of this pressure gradient, which is about 0.7% of the dynamic head, is treated as a pressure gradient across the balance, it would lead to a 10% uncertainty in the skin friction measurement. We have not been successful in measuring the pressure within our balance gaps, perhaps because of our relatively small balance sections, but this measurement has been successful elsewhere and is certainly worth the effort.

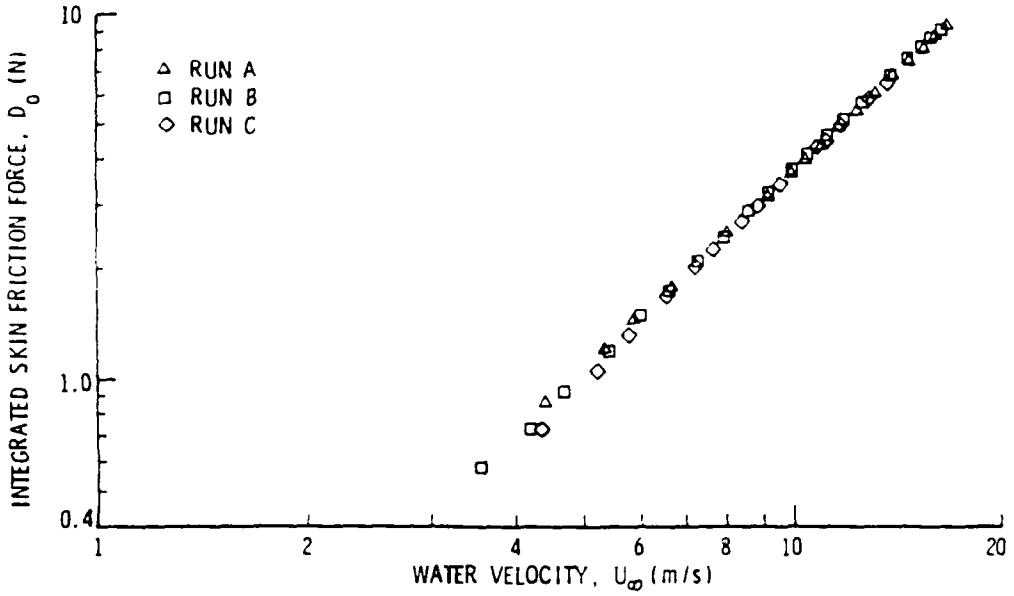

Figure 20. Shear Stress Balance Performance Showing Sensitivity and Linearity

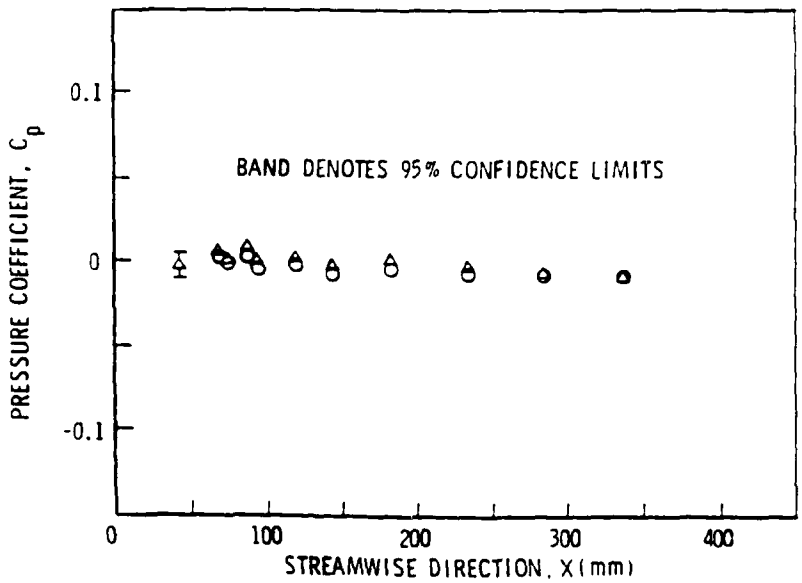

Figure 21. Typical Pressure Gradient Over a Flat Plate Mounted in a Water Tunnel

Because we have used our balance sections in nominally zero pressure gradient turbulent boundary layers, a check on their performance is available by a comparison with existing data correlations. A comparison of some of our data against a correlation given in White (1974) is shown in Fig. 22. The fit to the correlation depends on a choice of virtual origin for the experimental data. This is often fixed by a trip wire or a leading edge condition or by an extrapolation of the data to zero displacement or momentum thickness. For our results, it is comforting to know that a ten percent error in virtual origin results in only a 0.8% error in the skin friction.

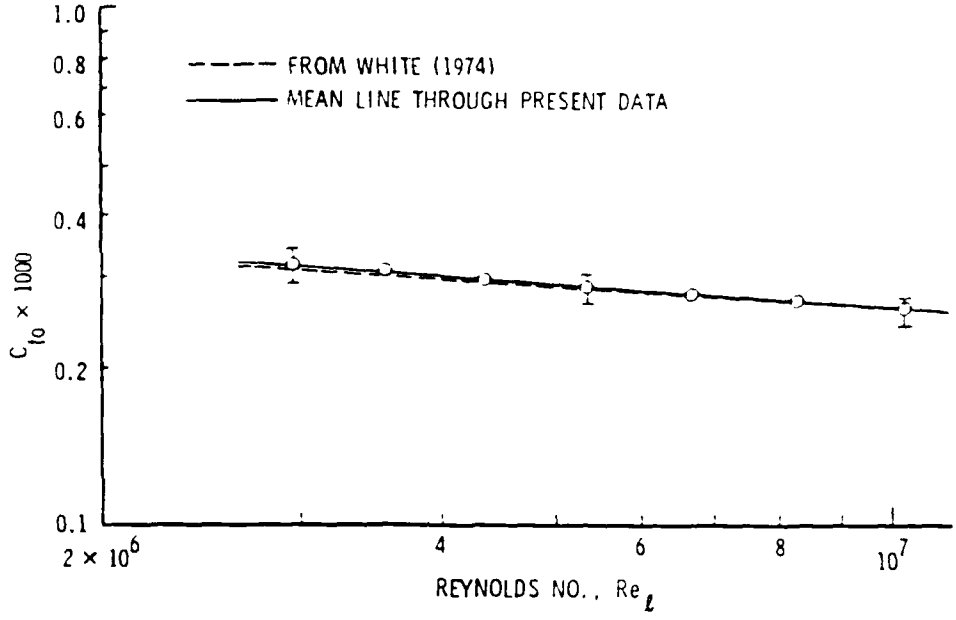

Figure 22. Skin Friction Coefficient on a Flat Plate Showing Comparison of Water Tunnel Data with Theory

Misalignment of the balance can cause extraneous pressure effects and significant errors in skin friction. In boundary layers with very small inner regions these effects can be seen for even very small misalignments, i.e. on the order of 25 microns. Results from a systematic study are shown in Fig. 23. Clearly it is better to err in the direction of a recessed element.

To obtain information about the local time dependent behavior of these turbulent boundary layers we have generally relied on flush-mounted hot film probes and LDV. For opaque microbubble flows, for example, the flush mounted films provide our only means of measuring the time dependent nature of the flow. The theory of operation of these probes can be traced back to the work of Ludweig (1950), Ludweig and Tillmann (1954) and Liepmann and Skinner (1954) and shows that the wall shear stress (τ_w) is related to the measured voltage (E) through

$$E^2 = A\, \tau_w^{1/3} + B. \qquad (4.1.1)$$

---

[1] Figures 20-27 have been reprinted from the Ph.D. thesis of Madavan (Penn State University, 1984).

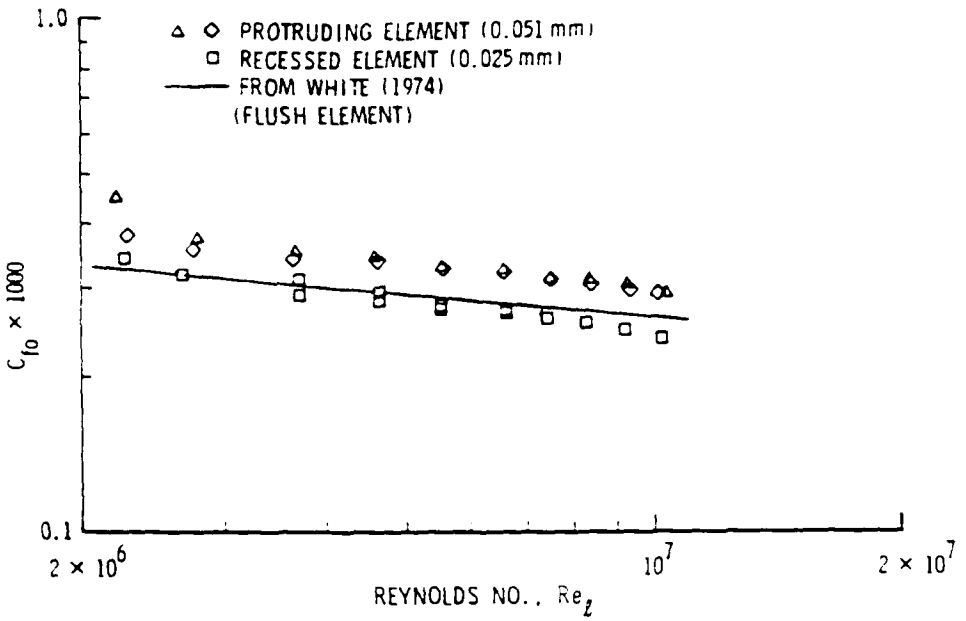

Figure 23. Effect of Shear Balance Misalignment on Skin Friction Coefficient Measured on a Flat Plate Mounted in a Water Tunnel

where the coefficients A and B must be found through calibration against a known flow. Experimental evidence shows (for example, Bellhouse and Schultz, 1966) that a relationship of the same form exists for turbulent flows provided that the thermal boundary layer which grows on the probe lies entirely within the viscous sublayer. Of course, for a turbulent flow the equation relates instantaneous values of the shear stress and the measured voltage.

For all our water tunnel experiments we have been fortunate enough to have sufficient boundary layer data to permit us to calibrate these hot film probes in place. Our experience in the use of these probes in other types of measurements indicates that with the small spatial scales involved in the flush-alignment, that calibration outside the facility used would lead to only order of magnitude results. Calibration in place implies calibration in a turbulent boundary layer and Sandborn (1979) and Hanratty and Campbell (1982) have recommended an interactive technique toward the determination of the constants A and B. In our measurements we have found the initial estimate of the constants from the mean calibration data to be sufficiently accurate. A typical hot film calibration curve is shown in Figure 24. The fit of two straight lines, with a higher slope to the data at lower tunnel speed, is usual and is probably a result of free convection effects at low speeds.

The "miniature" hot film probes we employ are not small when compared to our inner boundary layer scales. Active sensor elements have a streamwise width of 400 microns by a cross-stream dimension of 900 microns. The probes then are some 10 to 80 sublayer thicknesses in streamwise extent with an L/D ratio of 2.25. With streak spacing estimated as roughly 100 wall units (20 sublayer thicknesses) the probes may be averaging over as many as 4 wall layer streaks. One might suppose that the effect

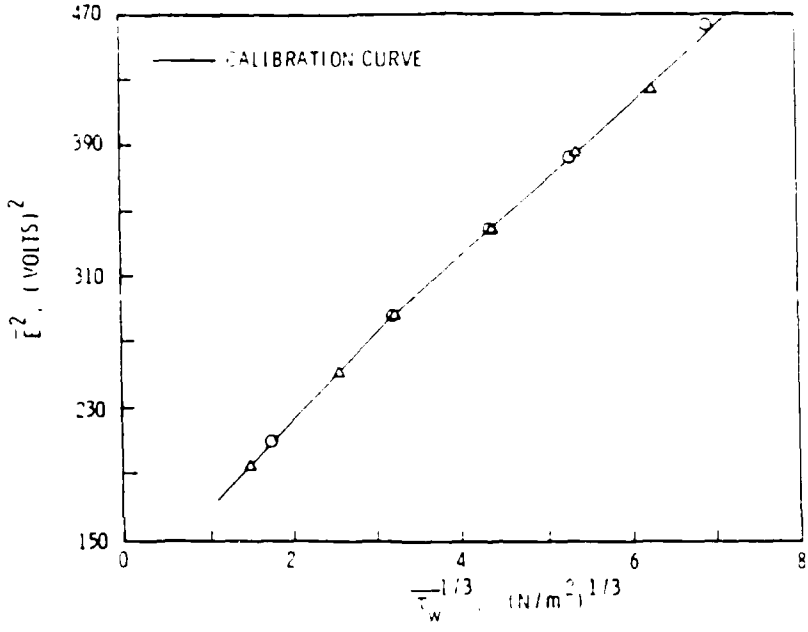

Figure 24. Typical Calibration of a Flush-Mounted Hot Film Probe

of this averaging would appear in plots of the intensity of shear stress fluctuations, which we show versus Reynolds number in Fig. 25. In Fig. 25, the dotted line represents data taken from Eckelmann's study in the thick viscous sublayer of an oil channel. Scatter in the measurements is typical of results taken from several different probes and may be related to the relative success in flush mounting the individual probes. Eckelmann (1974) notes that his value of 0.24 agrees well with the extrapolation of Laufer's hot wire measurements to the wall. Others, most notably Hanratty and his colleagues, find values closer to 0.32-0.36. While the current paper was in review, Alfredsson et. al. (1988) published an attempt to explain the large variation of intensities obtained by various researchers. They conclude that the intensity value should be close to 0.4, and that the results presented in Fig. 25 do indeed suffer from spatial averaging.

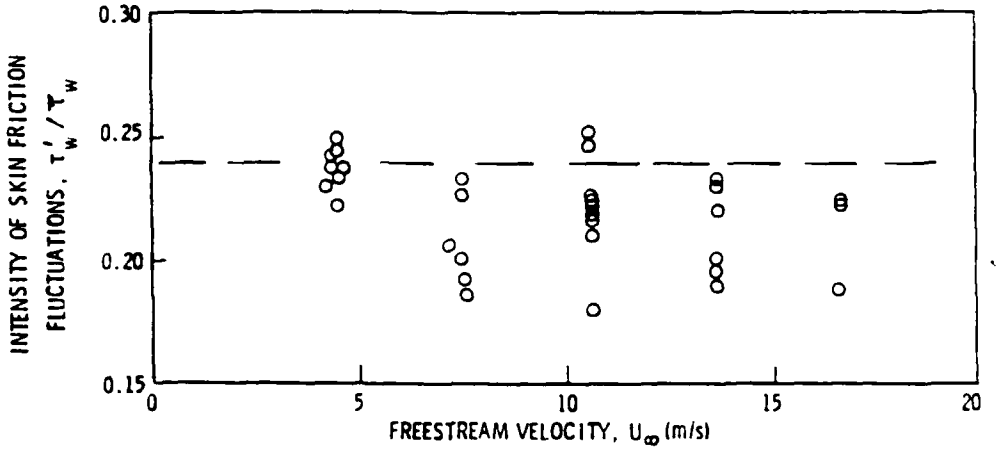

Figure 25. Typical Measurements of Fluctuating Wall Shear Stress Using Hot Film Probes

LDV measurements in high Reynolds number liquid boundary layers are also restricted by problems of small inner-scale size. Using standard backscatter optics, an argon-ion laser at 488 nm (or 512 nm) a 3.75x beam expander, and a 480 mm lens, our ellipsoidal measuring volume is 80 microns in the vertical and streamwise direction and 580 microns in the cross-stream direction. Our measurement volume then is 10 to 80 wall units in the vertical direction with an L/D of 6. Typical plots of mean velocity and turbulence intensity are shown in Fig.'s 26 and 27, respectively. Even with tilting the laser beams at some small angle to the plate to decrease reflections, y+ values of less than 30 are quite unusual to obtain[2]. Turbulence production, by way of comparison, may peak near a y+ of 15.

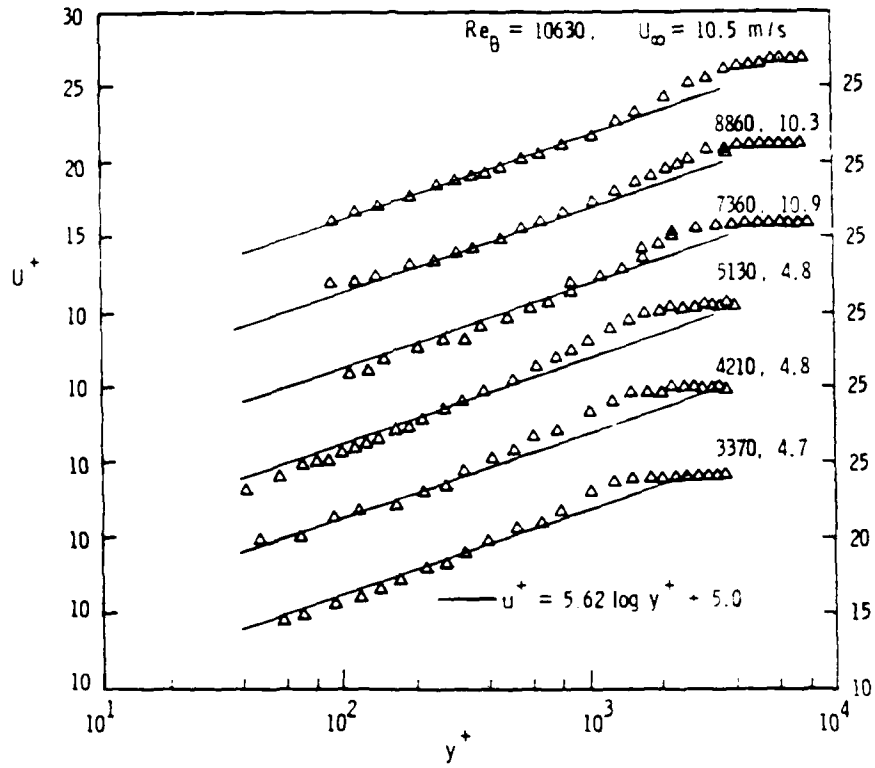

Figure 26. Laser Doppler Velocimetry (LDV) Measurements of Turbulent Boundary Layers on a Flat Plate

In summary, we have described some of our more successful measurement techniques for high-velocity turbulent water boundary layers. These experiments have the singular difficulty of very small inner scales. Because of these small scales, the measurements we would most often like to make are simply not obtainable; some measurements we do make are often not as accurate as we would like.

4.2 Transitional Boundary Layers

Much of our recent experience in transitional boundary layers has come from our

[2] That is, for a flat plate boundary layer. We have managed to come significantly closer on axisymmetric bodies by exploiting the curvature of the body to reduce reflections.

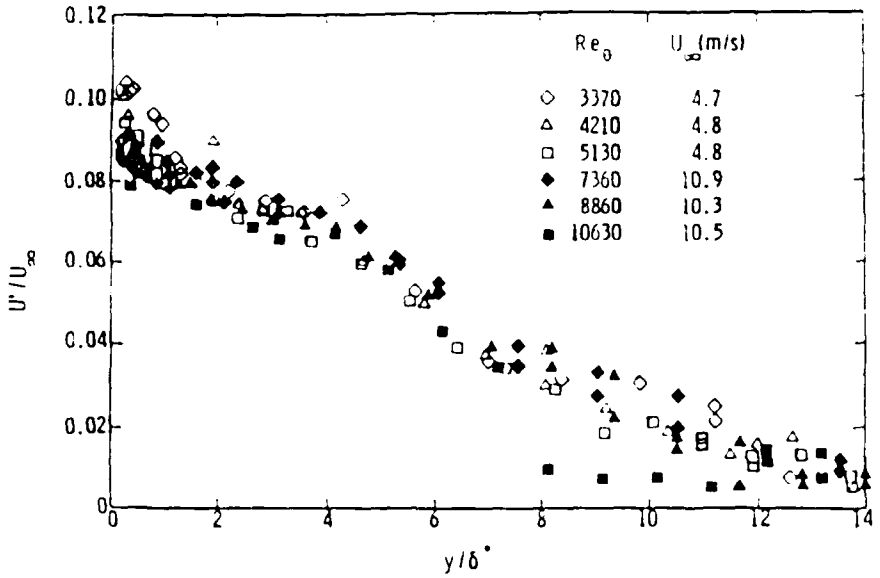

Figure 27. LDV Measurements of Turbulence Intensity (Streamwise Component)

work in heated laminar flow on underwater vehicles, again at large unit Reynolds numbers (Lauchle and Gurney, 1984). The object of the research was to achieve laminar flow at very large length Reynolds numbers by using surface heating to stabilize the boundary layer. The body employed was a 3.05 m long X 0.32 m diameter axisymmetric body and was tested in the large (1.22 m diameter) water tunnel. We found that with sufficient heating we could increase the length Reynolds number for transition from a cool wall value of 4.5×10^6 to a value near 37×10^6.

The laminar boundary layers that were encountered on this body were typically too small to permit velocity profile measurements, particularly for the heated cases. At 1.92 m from the nose, for example, the displacement thickness is about 2.33 mm, while at the same location with high heating (75 kW) the displacement thickness is only 100 microns. Our chief instrumentation has been flush-mounted hot film probes and injected dye-flow visualization. We found early on in the experiments that injection of fluid, at a low rate, did not interfere with the transition process, so that we could, by using dye, visualize it. This was very useful, particularly in determining at what position on the body the initiation of turbulent spots began. We found this position to be consistently at the predicted critical point of the body for the given level of heating. Heating increases the distance to the critical point. A typical visualization, which illustrates the spot formation is shown in Fig. 28.

We used flush mounted hot film probes to provide quantitative data on intermittency and burst rates. This is an ideal use for these probes as they may be run uncalibrated. We used probes at a fixed location (2.12 m downstream of the nose) so that the Reynolds number was varied by changing the mean tunnel speed.

---

[3] Typically we filter at 50 Hz. This is important if one wishes to have an intermittency detector with long time stability.

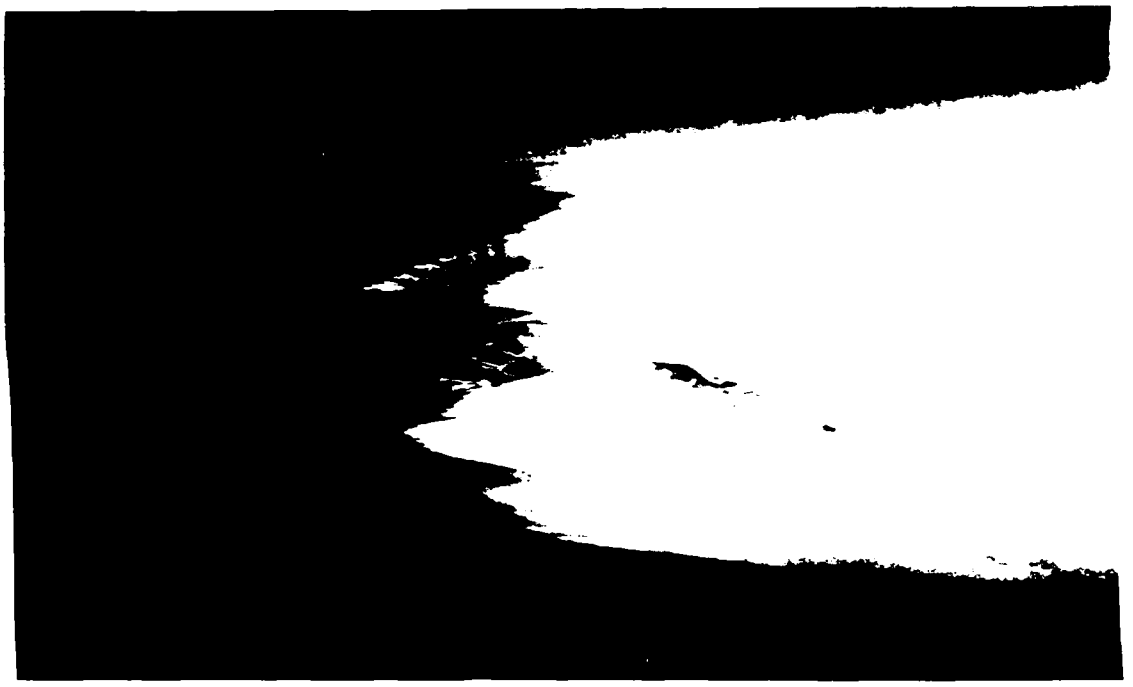

Figure 28. Flow Visualization of Natural Transition on a Heated Body Operated in a Water Tunnel

Transitional flow is intermittently turbulent and is generally described statistically through the intermittency function (γ) and the burst formation rate (N). We use an indicator function, I(t), which is set to zero for laminar flow and to one for turbulent flow, and define the intermittency as the time average value of the indicator function. An intermittency detector is used to generate the indicator function. First the hot-film signal is high passed filtered to remove low frequency information[3]; second it is differentiated to highlight the remaining high frequency fluctuations; third it is integrated with a short-time-constant low pass filter to smooth the fluctuations within the turbulent burst; and fourth the conditioned signal is passed through a variable threshold Schmidt trigger. The output of the Schmidt trigger is the indicator function. The intermittency is obtained by passing the indicator function through an integrating voltmeter, while the burst frequency is obtained by passing I(t) through a counter that only triggers on the leading edge of a step function. The threshold level of the Schmidt trigger is set by observing simultaneously the raw hot film signal and indicator function on a storage oscilloscope. Adjustments are made until I(t) tracks with the bursts sensed by the film. Typical intermittency and burst rate plots for no surface heating and substantial surface heating are shown in Fig. 29. Here, the arc length Reynolds number is based on the fixed arc length location of the probe (s = 2.12m).

Ladd and Hendricks (1985) have measured boundary layer transition on an ellipsoidal-shaped heated body which operated in the Naval Ocean Systems Center (NOSC) 0.305 in diameter water tunnel. This tunnel is capable of speeds up to 14 m/s with turbulence intensities reported to be 0.16 percent. The maximum transition Reynolds

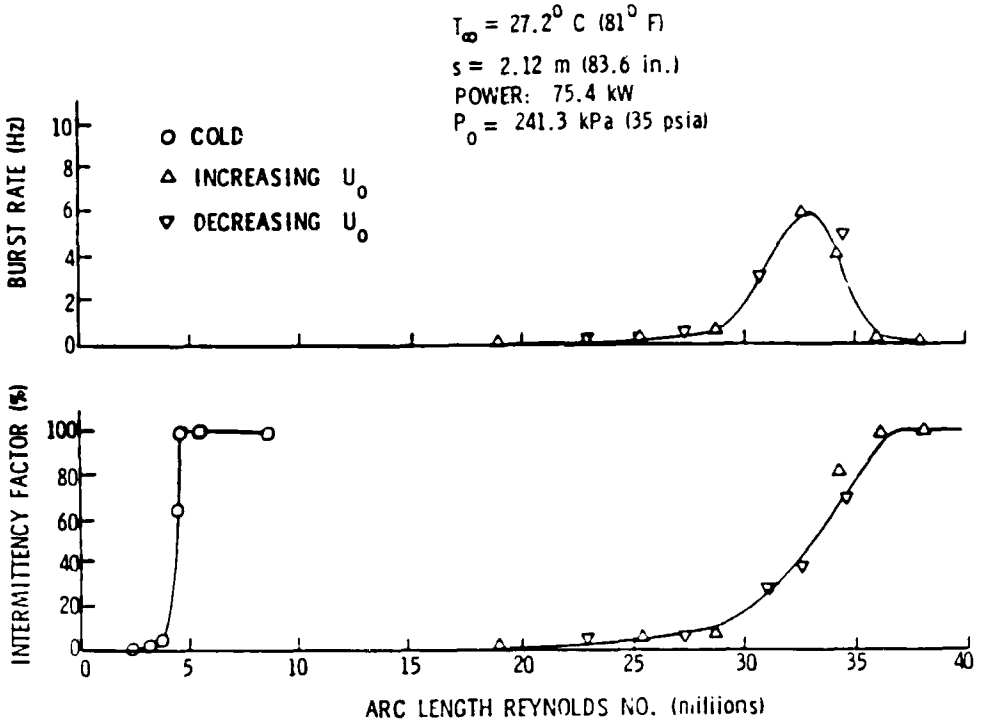

Figure 29. Transitional Boundary Layer Data Showing Spot Formation Rate and Intermittency on a Heated Underwater Body

number considered in their experiments is 7×10^6 (based on axial distance to transition). Intermittency in the transition zone was measured by locating the center of an LDV measuring volume at a distance of 5.8 θ away from the model wall, where θ is the computed laminar boundary layer momentum thickness. This distance was selected because it assures that the LDV measuring volume is outside of the region of "sharp" velocity gradient. They found this necessary to avoid the effects of the finite measuring volume diameter (0.12 mm) and the sporadic characteristic of LDV signals, which would produce a fluctuating velocity output signal indistinguishable from turbulence, even in a fully laminar flow.

The laser scattering seeds used in the NOSC experiments were 1.5 μm silicon carbide particles. The LDV photodetector signal was processed with a counter-type processor that yields a voltage proportional to velocity. This signal was processed on a computer where software was provided to form the intermittency function, I(t). The threshold velocity selected to indicate a turbulent event was 10 percent of the maximum velocity fluctuation observed in the transitioning boundary layer. This is consistent with the Lauchle and Gurney (1984) experience using flush-mounted hot films and analog processing.

In transition experiments where intermittency is measured, 50 percent intermittency is usually selected to define the transition point or transition velocity.

5.0 MULTIPHASE FLOW MEASUREMENTS

5.1 Multiphase Flows

There are many different techniques associated with the measurement of multiphase flows (i.e. liquid-solid-gas flows) due to the great variety of flows themselves. Accurate measurements of the fundamental physical quantities are not only an essential part in an understanding of multiphase flows but also in the measurement process itself. Almost all flow visualization techniques involve measurement processes having multiphases. Even the early work of Osborne Reynolds, a 19th-century English scientist, utilized dye to visualize pipe flows. Today, optical techniques such as laser velocimetry and pulsed velocimetry (Dybbs and Pfund, 1985) involve the measurement of solids in a fluid and problems of particle velocity fidelity arise as well as statistical particle bias problems.

There have been many international symposia and journal articles directed toward flow visualization techniques and multiphase flow measurements. For example, the American Society of Mechanical Engineers-Fluids Engineering Division sponsors annually The Cavitation and Multiphase Flow Forum (see Furuya 1987) and Fluid Measurements and Instrumental Forum (see Bajura and Billet, 1986) that serve as a source of information and provide valuable insite into multiphase flow measurements. Although the applications are very diverse, the use of optical measurement techniques does appear to be one common denominator in multiphase flow measurements in high-Reynolds number liquid flow facilities.

Multiphase flow measurements in the flow facilities at ARL Penn State have for the most part been developed to understand the basic fluid mechanics of cavitation. Cavitation is the gas-liquid region created by a localized pressure reduction produced by the dynamic action of the fluid in the interior and/or the boundaries of a liquid system. Cavitation will occur in the lowest pressure regions of the flowfield. Figure 30 shows cavitation occurring in a pump stage. A first order measure of cavitation is determined from the cavitation number defined as

$$\sigma = \frac{P_\infty - P_v}{1/2\ \rho\ V_\infty^2} \qquad (5.1.1)$$

where P_∞ is the reference static pressure, P_v is the vapor pressure at the bulk temperature of the liquid, ρ is the liquid density at the bulk temperature of the liquid and V_∞ is a reference velocity. Thus from a classical point of view, cavitation inception occurs when the cavitation number is equal to the absolute value of the local minimum pressure coefficient. At higher values of cavitation number no cavitation can occur and at lower values of cavitation number developed cavitation will occur.

In order to determine cavitation inception, the cavitation number is obtained by either varying the static pressure at constant velocity or varying the velocity at

Figure 30. Photograph of Cavitation.

constant pressure. In either case the condition is identified by the observation of large bubbles or by acoustic sensors through the noting of an increase in noise level. Figure 31 shows the characteristics of cavitation noise, and cavitation inception can be noted where a rapid increase in noise level occurs for a small variation in cavitation number. Broadband noise is created as the bubbles collapse in a high pressure region. A description of cavitation noise theories can be found for example in Blake (1987) and Hamilton, Thompson and Billet (1986).

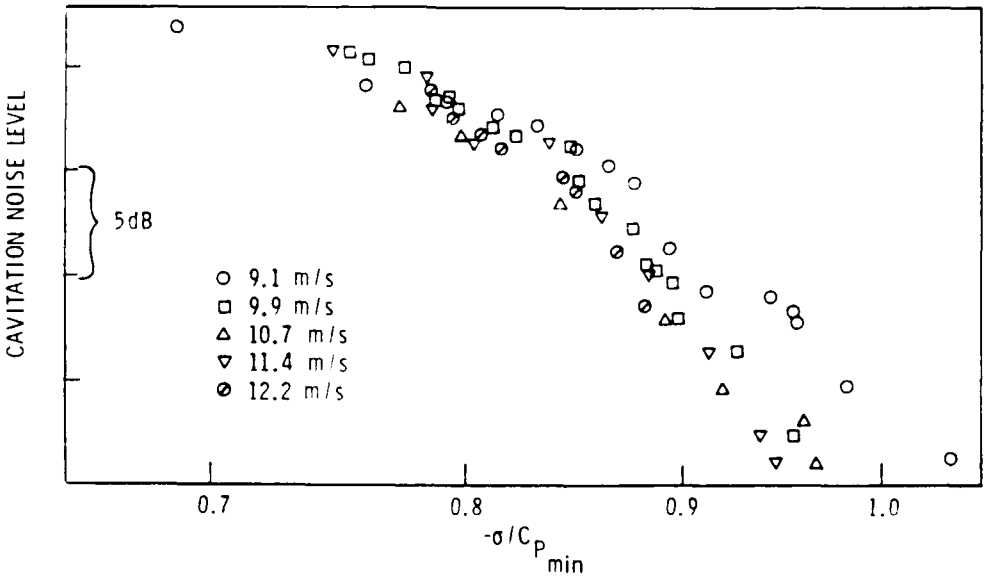

Figure 31. Cavitation Noise.

Departures from the classical viewpoint of cavitation are due to so-called scale effects (see Holl, 1969) and are (1) due to variations in the local pressure field from the perfect fluid model, and (2) bubble dynamics which cause the pressure at inception of the microbubble to vary from equilibrium vapor pressure. Thus, cavitation measurements generally involve fluid measurements, cavitation bubble measurements, and cavitation nuclei measurements.

Past research studies have included such diverse measurement techniques such as oil-paint film, tufts, dyes, bubble tracing, photography, and Schlieren photography. Now X-rays, gamma rays, radio and lightwaves, and computer technology are combined in complex systems for these measurements. Emphasis at the ARL/Penn State has been on developing electro-optical techniques such as laser velocimetry, laser light-scattering, and holography. The application of these techniques is essentially due to two fundamental properties; it is non-intrusive, and in general, gives directly the measurement of the flow quality. As an example, the instantaneous components of the local velocity vector can be obtained with a laser velocimeter and holography gives directly the size and distribution of bubbles.

A summary of laser velocimeter and its application to water tunnel measurements is given in Billet (1987). Obviously, the major problem with these systems is optical access to the measurement location which is not always easy in a high-speed water tunnel.

5.2 Cavitation Nuclei Measurements

Cavitation nuclei is a general term used to refer to the impurities that cause weak spots in liquids and thus prevent the liquid from supporting higher liquid tensions. The importance of cavitation nuclei has been noted as early as a century ago by Besant (1859). A relationship between nuclei size and cavitation growth has been established by a bubble dynamics model started by Lord Rayleigh (1917) almost half a century ago followed by the work of Plesset (1949) and others. The importance of nuclei size and distribution has also been shown by many experimental efforts. Recently, the results of experiments conducted by members of the International Towing Tank Conference (ITTC) (see Lindgram and Johnsson, 1966 and Acosta and Parkin, 1970) have provided impetus for attempts to quantify a relationship between nuclei and cavitation. As a direct result, many different measurement techniques have been developed and a summary of many techniques is given by Billet (1986) and in Fig. 32.

Two significantly different approaches to measuring cavitation nuclei have been developed. One is to measure the particulate/microbubble distributions by utilizing acoustical (Schiebe and Killen, 1971 and Medwin, 1977), electrical (Hammitt, et.al., 1974 and Oba, 1981) or optical techniques (Keller, 1972, Farmer, 1976, Gates and Bacon, 1978 and Gowing and Ling, 1980). The other approach measures a cavitation event rate for a liquid under various tensions and establishes a cavitation susceptibility (Oldenziel, 1979, Lecoffre and Bonnin, 1979 and d'Agostino and Acosta, 1983).

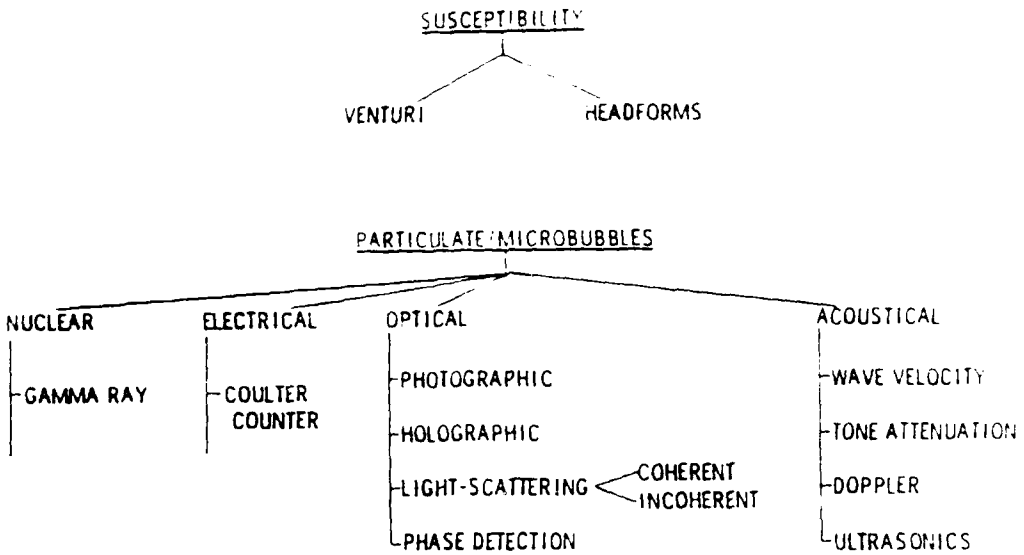

Figure 32. Cavitation Nuclei Measurement Techniques.

The most widely used method of establishing cavitation susceptibility utilizes a venturi system. Measurements of cavitation susceptibility are based on bubble events that occur in a prescribed pressure field. A small venturi tube made of glass (Oldenziel, 1979) or steel (Lecoffre and Bonnin, 1979) is used and the minimum pressure can be varied by a adjusting the volume flow rates. The number of cavitation events can be determined optically or by recording the noise generated by their collapse in a downstream diffuser. The corresponding concentrations of unstable nuclei can be estimated from the pressure at the throat and the count of cavitation bubbles. A schematic showing the principles of operation is given in Fig. 33.

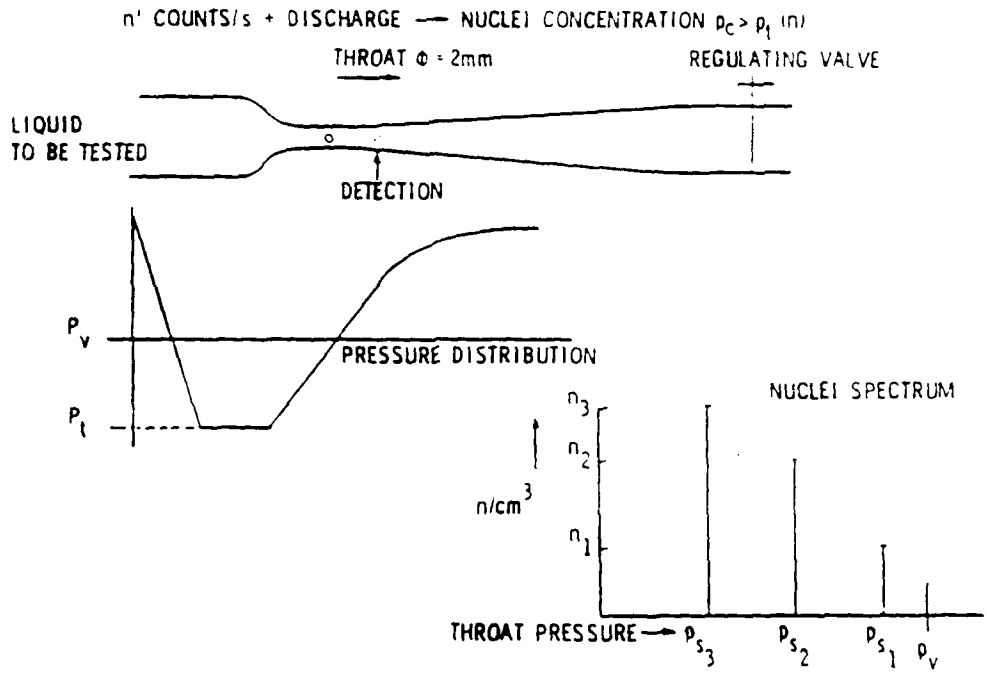

Figure 33. Venturi System.

The venturi system can be severely limited by nuclei concentration larger than 10 cm^{-3}; however, it can provide a direct measure of both the liquid critical tension and nuclei concentrations over a very large size range. Shen and Gowing (1985) and Chahine and Shen (1985) discuss the calculation of bubble dynamics in the throat of a venturi. A more general discussion of cavitation susceptibility meters is given by d'Agostino and Acosta (1983).

Light-scattering techniques are the most widely used methods to determine nuclei distributions. In some cases, the amplitude of the scattered light is related to the size. Other methods are based on laser doppler techniques in which particulate visibility or phase of the doppler frequency is correlated with size. One of the first applications of a scattered-light method to measure nuclei distributions in a water tunnel was done by Keller (1972) and utilized a laser as a light source.

A light-scattering system developed for water tunnel applications at ARL/Penn State utilizes the laser light-scattering principles and is shown schematically in Fig. 34. This system is based on the relationship between the radius of a scattering sphere and the scattered intensity. A comparison between experimental data and Mie theory is given in Fig. 35.

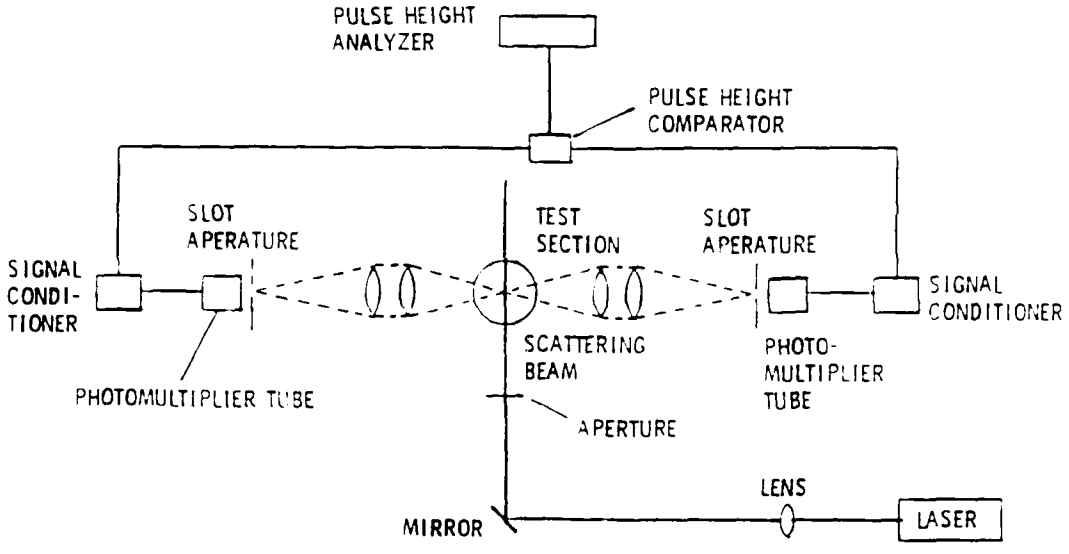

Figure 34. Light-Scattering System.

An on-line method was developed to discriminate between the light scattered from microbubbles and particulates. An analytical investigation by Kohler and Billet (1981) showed that the asymmetry of a particulate relative to the postulated spherical symmetry of a microbubble results in a scattered field that is quite different. Yungkurth (1983) conducted a series of tests in a water tunnel that showed that discrimination using this theory is only possible when the particulate population is less than the microbubble population.

The largest classifying error of this technique is the tendency for spherical microbubbles of a given size to register a number in not only the classification channel corresponding to that size, but also in all channels lower than that size.

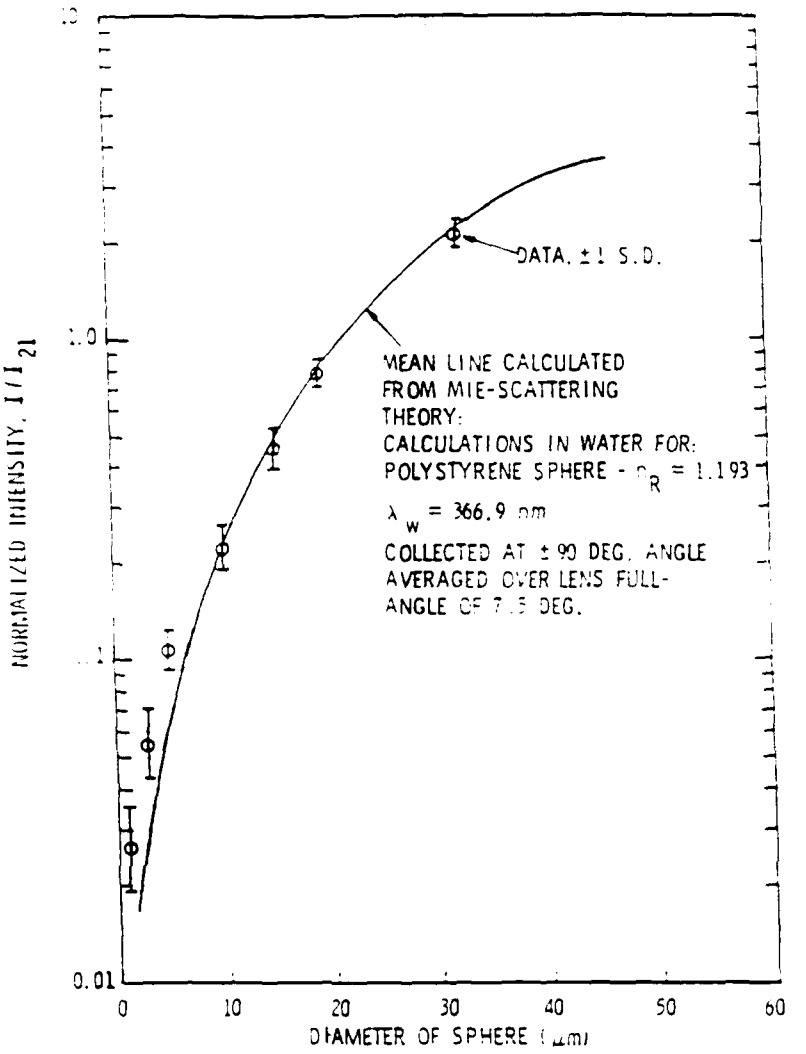

Figure 35. Comparison Between Calculated and Measured Scattered Intensities for Spheres in Water.

This is due to the probe volume having a nonuniform light intensity. Fig. 36 shows the different light scattering characteristic of the same size bubble located at different locations within the laser beam.

This experimental result shows that the count histogram does not reflect directly the actual distribution of sizes present. The amplitude of the voltage pulse (A) produced by a photomultiplier as a result of a microbubble entering the measuring volume can be expressed as

$$A = G \frac{\lambda^2}{4\pi^2 r^2} I(x,y)\, F(\alpha,\Omega,\eta_{rel}) \quad . \qquad (5.2.1)$$

where G = gain of associated electronics

λ = light wavelengths

r = effective optical distance

$I(x,y)$ = intensity of light beam in probe volume

$F(\alpha, M, n_{rel})$ = scattering response function.

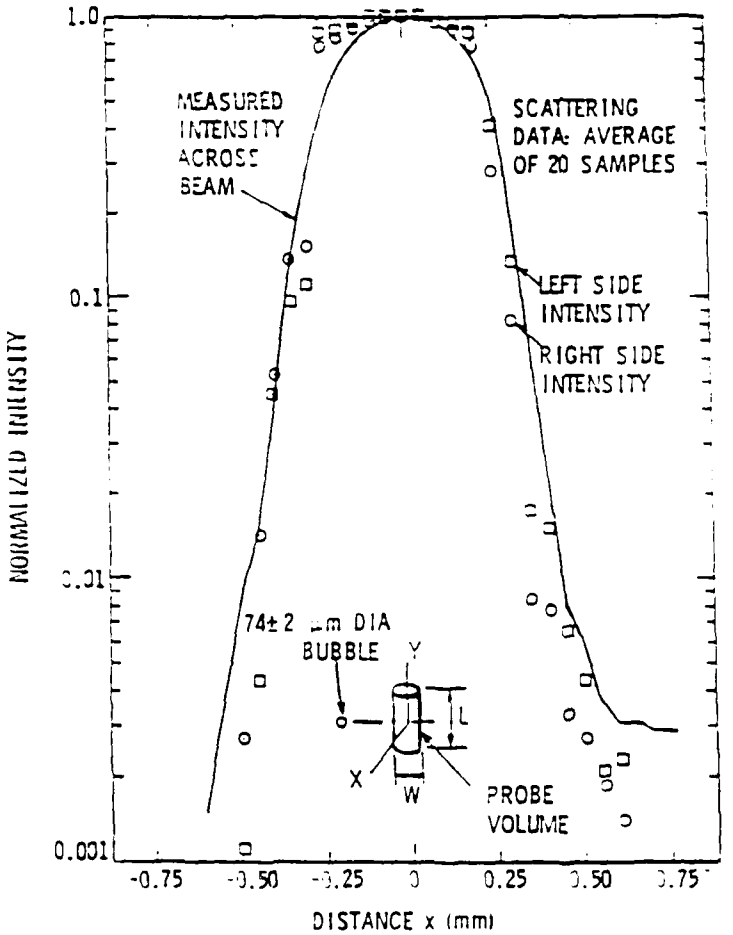

Figure 36. Normalized Maximum Scattered Intensity of a Bubble Along the Axis Normal to the Light Beam.

To correct for this, an inversion scheme that accounts for the nonuniform light intensity has been developed. Thus the above equation can be generalized in terms of discrete classification channels as

$$C_i = U \Delta S_{ij} N_j \qquad (5.2.2)$$

where U is the bulk velocity of the flow, C_i is the column matrix of detected count rates ΔS_{ij} is the equivalent cross-sectional area of the probe volume for the microbubble response function F_j, and N_j is the column matrix of detected count rates.

It is important to note that the S_{ij} elements are simply probabilities based on the light intensity distribution and the width of the classification channel. The actual data received in an experiment are the C_i collected in the various channels. The

information desired is the microbubble density, N_j, thus the above equation can be written as

$$N_j = \frac{1}{\bar{U}} C_i \, \Delta S_{ij}^{-1} \quad . \qquad (5.2.3)$$

where ΔS_{ij}^{-1} is the inverse of the matrix ΔS_{ij}. Thus the microbubble density for one channel is actually a weighted sum of the count rates from every channel.

Even utilizing an inversion procedure to account for the nonuniformity of the light intensity, the question of system accuracy cannot be answered.. The system requires an appropriate statistical sample before the inversion procedure can account properly for the nonuniform light intensity.

A computer model of the probe volume - microbubble distribution - inversion procedure interaction has been developed and details are given in Billet (1986). The results clearly show the importance of the size width of the classification channels and of the sample size. A comparison of microbubble distributions obtained with the light-scattering system and by using holographic techniques is given in Fig. 37.

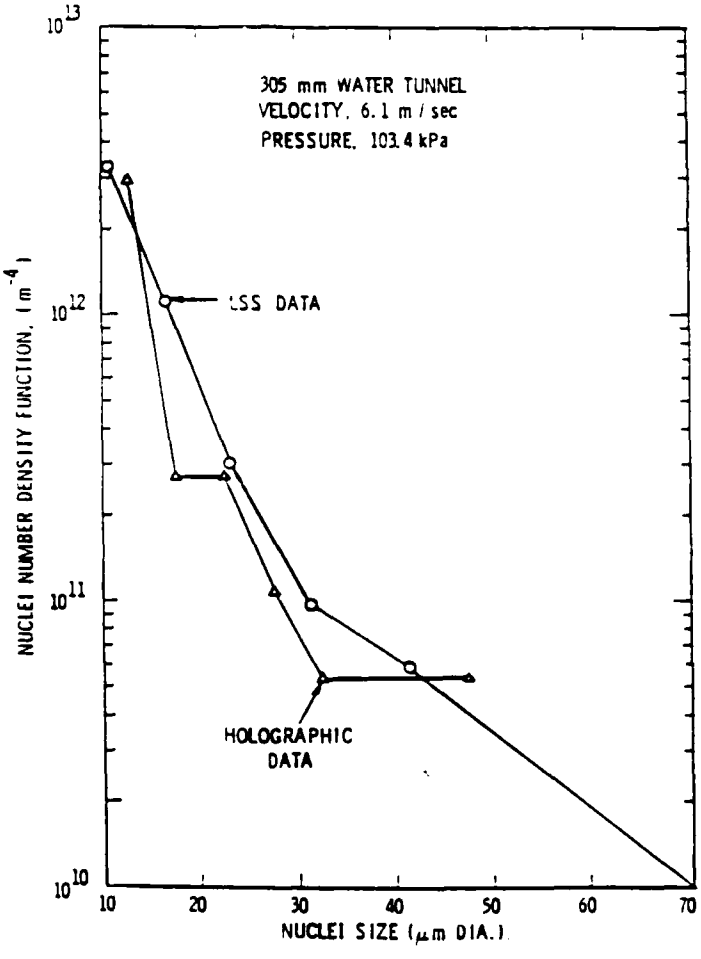

Figure 37. Number Density Data for V_∞ = 6.1 m/sec, P = 103.4kPa in 30.5 cm Water Tunnel.

5.3 Cavitation Bubble Measurements

Holography is utilized to record the growth of cavitation bubbles, the trajectory of microbubbles and the size and concentration of cavitation nuclei. Holography is a complete measurement technique that makes possible the recording of color, scale and three-dimensional images of the multiphase flow. Unlike an ordinary photograph or a Schlieren photograph, which record only two-dimensional images, a hologram preserves the three-dimensional information by recording the wave front phase differences as well as light intensity. When a coherent light beam encounters a gas bubble or some other change in the refractive index of the medium, the phase of the light waves is modulated. Scattered coherent light encodes all the optical properties of the object.

In the holographic process, a laser beam is split into two separate beams - one that illuminates the object and the other which is a reference beam superimposed on the light field scattered from the object, Fig. 38a. The interference pattern generated by these beams is recorded in a transparent light-sensitive emulsion. Development of the exposed emulsion produces a hologram that contains the complete optical information.

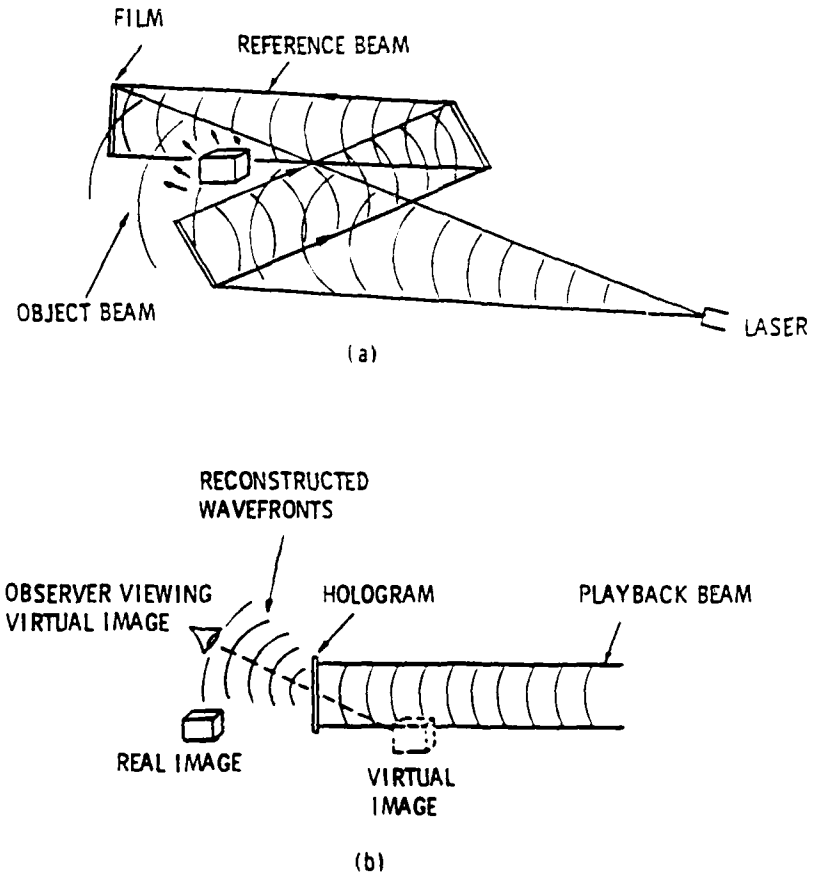

Figure 38. (a) Hologram Recording.
(b) Wavefront Reconstruction for Image Playback.

The hologram is composed of a series of light and dark fringes on the transparent substrate. When a laser beam illuminates it at the same incidence angle as the original reference beam, the light is diffracted by the fringes. Converging and diverging wavefronts, similar to those scattered by the object are reconstructed (Fig. 38b). The diverging wavefronts appear to come from a virtual image, visible from behind the hologram. This image, seen through the hologram, appears to be at the location of the original object. The converging wavefronts form a real image of the object on the opposite side of the hologram.

Two holographic configurations are used for cavitation research in the water tunnel. An off-axis system has spatially separated object and reference beams. The term off-axis indicates that the beams are not coincident along a single axis. An in-line system used one beam as both the object beam and the reference beam.

In-line holography is a very well established technique for the study of microbubbles in a dynamic situation. Although the technique is almost as old as modern holography, it is still one of the most reliable measurement methods. Consequently, research to improve different aspects of the method are continuing, e.g., Vikram and Billet (1982), (1983), (1984).

In-line holography has a number of advantages for cavitation measurements. The limited window area and working space around a water tunnel test section provide little off-axis space for a separate reference beam. The in-line system has been used to successfully measure microbubble concentration as high as 200/cm^3 over a size range of 20-200 microns in the tunnel. Also, it is capable of obtaining bubble growth information via multiple exposures for bubbles having wall velocities as high as 100 m/sec. However, when more than 20% of the reference beam is distorted, an off-axis system is necessary and has been utilized to measure concentrations as high as 1500/cm^3 in the water tunnel.

The holographic system has three main components: the holocamera, a hologram recording system and a reconstruction system. Schematics are shown in Fig.'s 39 and 40. The holocamera utilized at ARL/Penn State is a double-pulse ruby laser Q-switched

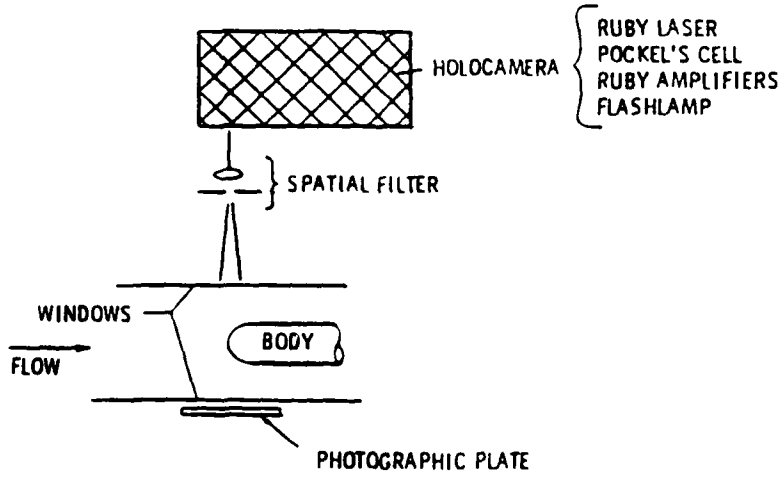

Figure 39. Three Main Components of an In-Line System.

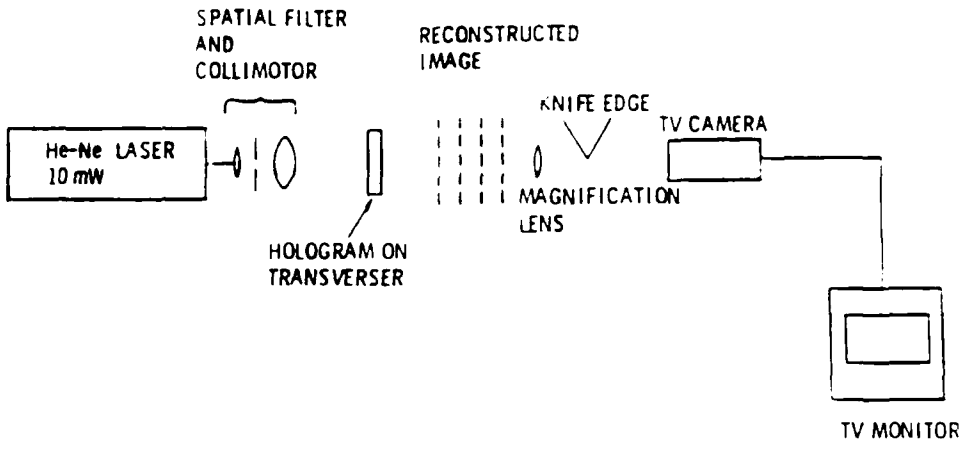

Figure 40. Holographic Reconstruction System.

with a Pockels cell. The power of the system is up to 10 joules in a single 20-msec pulse or two 20-msec pulses of 5 joules each. The pulse-repetition rate can be varied from 400 msec to about 1 msec. A resolution of 15 μm can be obtained when the central maximum fringe of the diffraction pattern is recorded with at least three side lobes. This also requires an allowable fringe movement of less than 1/40 of the fringe spacing.

6.0 HYDROACOUSTICS MEASUREMENTS

As noted previously, radiated noise generated by turbulent stresses depends on a high power of the Mach number. Even in a high-speed water tunnel the Mach number may be as low as 0.01; the flow is nearly incompressible, and the level of sound radiation is very low compared to air at the same Reynolds number. Nevertheless, hydrodynamically-generated sound does occur under water and its physical understanding and control is an important subject of past and current research projects.

The most efficient sources of hydrodynamic noise are cavitation and other multiphase flows. These sources are monopole and the sound level increases with the fourth power of Mach number. Such flows create noise that is usually more intense than the facility background noise which results in a good signal-to-noise ratio. Examples of cavitation noise measured in water tunnels may be found in Blake, et.al. (1977), Marboe (1982), Barker (1974), Gavigan, et.al. (1974), and Hamilton (1986).

Flow noise in single-phase flow is generated in both free and bounded shear layers. Turbulent boundary layer noise obeys a fifth to sixth power dependence on Mach number and is hence less efficient than cavitation noise. Its directivity is that of dipole radiation. Free-shear flows are quite inefficient sound radiators at low Mach numbers; the intensity scales with the eighth power of the Mach number and the directivity is described by quadruples. Boundary-layer noise can, under some instances, be measured in a water tunnel environment (Skudrzyk and Haddle, 1960, Lauchle, 1977 and Greshilov and Mironov, 1983), but difficulties in signal-to-noise ratio often invalidate the data. The problem of signal-to-noise ratio is compounded

in free-shear flows and no known noise data are reported.

The above discussion is concerned with the radiated noise associated with unsteady flows. The subject of turbulent wall pressure fluctuations is a different matter. These fluctuations are generally quite intense since they scale with the dynamic head and depend only secondarily on Mach number. Their measurement, at a point, in liquid flows have been somewhat successful and several studies are reported: for example, see Willmarth (1975) for a review, and Bakewell (1968), Barker (1973), Lyamshev, et. al. (1984), Kadykov and Lyamshev (1970), Skudrzyk and Haddle (1960), Lauchle and Daniels (1987), and Horne and Hansen (1981) for more specific studies involving liquid flow tunnels.

The radiation field from liquid stress fluctuations is non-dispersive and depends on only one wavenumber, the acoustic wavenumber. On the other hand, turbulent wall pressure fields are dispersive, being dependent on a wide range of characteristic velocities, and hence on a wide range of subsonic wavenumbers. Therefore, in measuring wall pressure fluctuations, one must be concerned with both spatial and temporal information.

A complete survey of such fields requires that measurements be made at many locations, simultaneously. These measurements are made using flush-mounted pressure transducers, the size of which is important. Large transducers tend to filter out the high wavenumber components, while small transducers give an average of the field over a large wavenumber range. In order to measure a turbulent fluctuation within some pre-determined wavenumber band, one must use an array of transducers, shaded appropriately to give the desired result. These arrays are called wavevector filters and are described by Maidanik and Jorgensen (1967). Several wavevector filters, each of a different design, must be used to cover a given broad wavenumber range. The difficulties of this approach are significant; successful measurements of the entire wavevector/frequency spectrum of turbulent boundary layer wall pressure fluctuations have yet to be reported for any medium. A predominant problem is facility background noise. This noise is capable of leaking into the side lobes of a wavevector filter and hence contaminating the desired data. The problem remains unsolved.

In the remainder of this section, methods for measuring the flow-induced radiation field and turbulent boundary layer wall pressure fluctuations in water tunnel testing will be high-lighted. The examples discussed will show new measurement procedures.

6.1 Radiated Noise Measurements

The water tunnel is not considered to be an ideal acoustic environment for making radiated noise measurements from a test object. The hard-wall construction of a typical tunnel results in internal sound fields that are highly reverberant. One can approach the problem by treating the tunnel as a reverberation chamber, calibrating it for its reverberation characteristics, and then using it to determine sound power (spatially-averaged sound intensity). This is the approach routinely used by Blake, et.al. (1977) in the DTRC 0.914 m water tunnel. The method does suppress the effects

of standing waves in the tunnel, but precludes the use of focused arrays or directional receivers to localize suspected noise sources. A second approach, used in the ARL Penn State 1.22 m tunnel, is to use individual receivers calibrated in situ. The receiver response is thus influenced significantly by the tunnel reverberation and one must be extremely careful is setting up the calibration. This requires some anticipation as to where the hydroacoustic sources of noise are situated in the actual test.

To illustrate the procedure, consider the directional hydrophone system shown in Fig. 41. The reflector is a pair of copper spinnings, welded at the edges, and filled with air. The air reflects sound underwater. A commercial hydrophone is placed at the focus of the ellipsoid forming the shape of the reflector. The other focus is in line with the tunnel centerline. Sound originating within the tunnel test section passes through the acoustically-transparent plexiglass viewing window of the tunnel hatch cover (Fig. 42), into the water-filled external tank, and is then sensed by the reflecting hydrophone. The reflector can be traversed up and down the length of the test section to help in isolating different sources of sound.

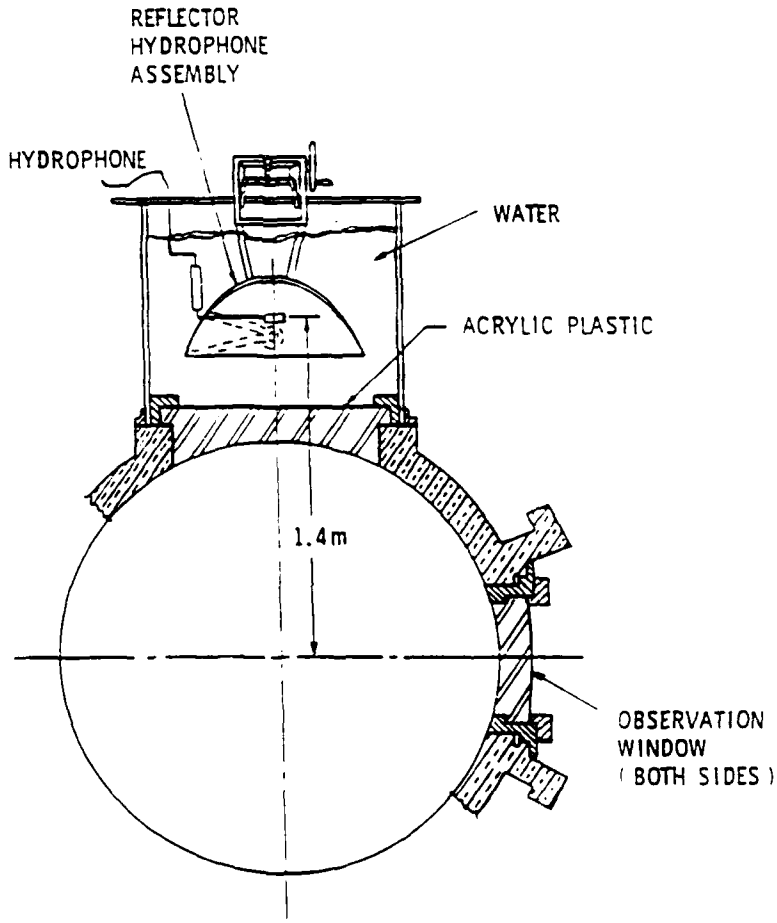

Figure 41. Schematic of the Reflecting Hydrophone System used on the 1.22 m ARL Penn State Water Tunnel

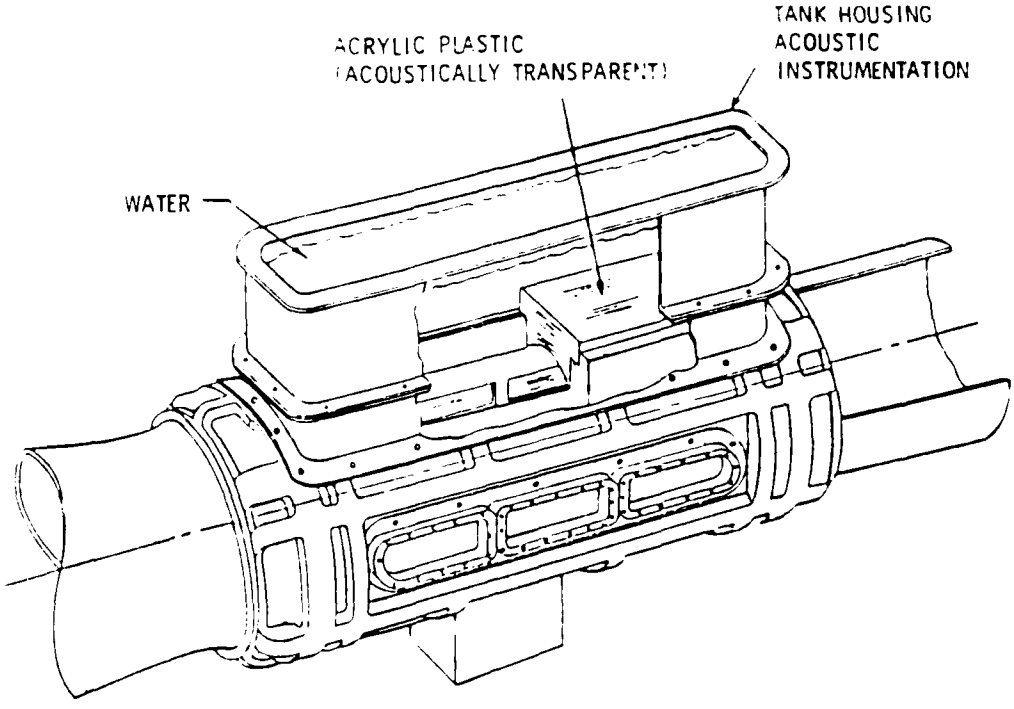

Figure 42. Overall View of the Acoustic Tank Mounted on the 1.22 m Water Tunnel.

The calibration procedure is to place a standard projector (piezoelectric hydrophone) at the anticipated location of the hydroacoustic source of interest. The transmitting frequency response of the standard must be know and is given as dB_S (referenced to 1 μPa - m/input volts). Typically, the sound output per unit input voltage at a fixed distance increases with frequency at 12 dB/octave. The projector is driven with broadband noise from a random noise generator. The mean-square level of this voltage is arbitrary but it must be measured by passing it through a spectrum analyzer. This level is called dB_X (re 1 volt). The raw output voltage from the receiver (dB_V re 1 volt) is also passed through the spectrum analyzer. The ordinate of this spectrum is then converted to sensitivity by:

$$dB_{M_O} = dB_V - dB_S - dB_X + 20 \log d, \qquad (6.1.1)$$

where d is the separation distance between source and receiver expressed in meters.

A typical sensitivity curve for the reflecting hydrophone is shown in Fig. 43. The tunnel was free of a test body and the projector was at the geometric center. Radial standing waves created in the test section are quite apparent in this sensitivity curve. The free-field sensitivity does not exhibit the rapid oscillation with frequency characteristic of the in-tunnel sensitivity. These oscillations are due to radial standing waves. The same waves are created when a broadband hydrodynamic source of sound (say a spot of cavitation) is situated at the same

location as was the projector in the calibration test. Then, through application of the sensitivity curve, these standing wave resonances (and anti-resonances) cancel: the reduced spectrum will be broadband and quite accurate.

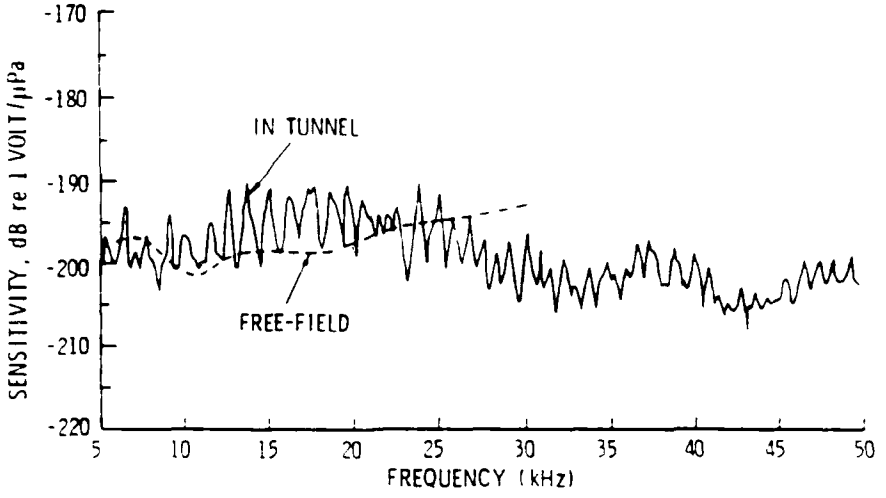

Figure 43. Reflecting Hydrophone Receiving Sensitivity

In many instances the hydrodynamic source of noise occupies a significant volume: for example, cavitating blades on a propeller. In these situations, the projector is placed at several locations within the source volume. The sensitivity curves measured for each location are then averaged together. The averaging eliminates much of the radial standing wave response and a fairly smooth sensitivity curve results.

With the projector at the test section center, a scan of the reflecting hydrophone results in data typified in Fig. 44. Based on the broadband data shown, the half-power beamwidth of the system is about 40 cm.

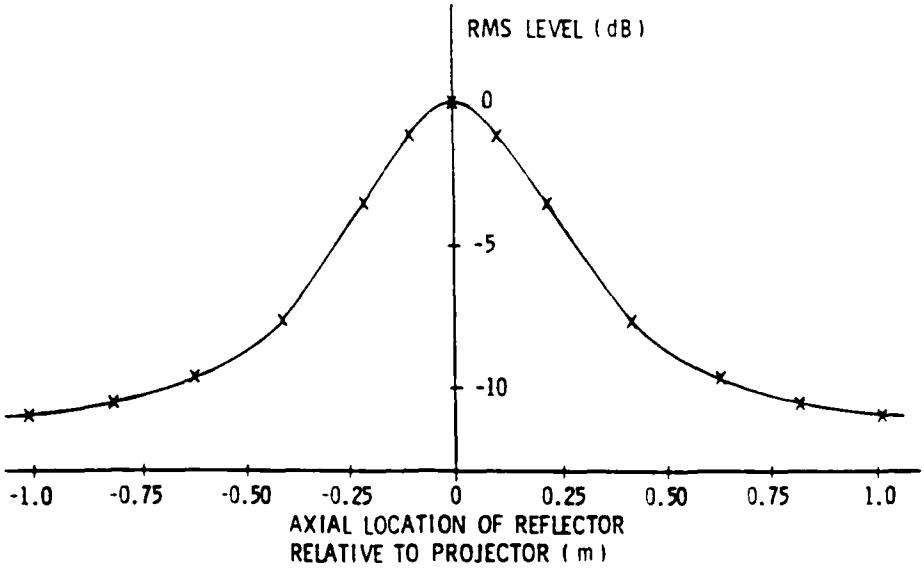

Figure 44. Typical Directivity of Reflecting Hydrophone

6.2 Volume Source Strength Measurements

Cavitation and other two-phase flows create omni-directional noise that is characterized by a random collection of point monopole sources. The time history of the acoustic pressure at distance r from a free-field monopole source is given by:

$$p(r,t) = \frac{\rho \ddot{V}(t-r/c)}{4\pi r} \quad . \qquad (6.2.1)$$

where ρ is the water density and $\ddot{V}$ is the volume acceleration of the source region evaluated at retarded time (c is the sonic velocity). The volume source strength is of fundamental importance in many radiation and scattering problems because it can be used in theoretical models employing various geometries and known Greens functions. Therefore, its measurement is of practical interest.

In principle, one could estimate the source strength of a cavitation source occurring in a water tunnel by the techniques given in Section 6.1. But those techniques break down at low frequencies where the acoustic wavelength becomes greater than the tunnel diameter. Then the back reaction of reflected waves on the known projector used during calibrations affects adversely the output of the projector (Waterhouse, 1958). This is why the data of Fig. 43 go no lower than 5kHz.

A method which alleviates this problem, while giving directly the acoustic source strength of cavitation in reverberant tunnel test sections, is now presented. The method is based on acoustic reciprocity and permits the determination of low-frequency volume source strength. Wolde (1973) first used the method for propeller cavitation studies, and later Bistafa (1984) used it for free shear flow cavitation noise produced by orifice plates. The method has an added benefit in that the actual acoustic measurements are performed with a microphone (in air) outside of the tunnel. This eliminates the use of hydrophones in the flow, or mounted in the walls of the tunnel, which can be influenced by other sources of noise. The cavitating orifice plate of Bistafa (1984) and Bistafa, Lauchle, and Reethof (1987) is used as an example.

The basis of the reciprocity technique is to establish a tunnel transfer function. Here, a sound projector is placed at some convenient location near the tunnel and the sound pressure is measured inside the tunnel (filled with water but with no flow) at the location where cavitation will occur during the test. A requirement is that the sound projector be reciprocal so that it can be used as the receiver during the cavitation test. A loudspeaker meets this requirement. Figure 45 depicts the two experiments, where the "direct" experiment is when cavitation occurs and $\dot{V}_2'$ is the volume velocity desired. The open-circuit voltage, e_1' of the speaker is measured in the direct experiment. In the "reciprocal" experiment, the speaker is driven with known current i_1'' and the pressure inside the tunnel is measured with an omni-directional hydrophone, p_2'' .

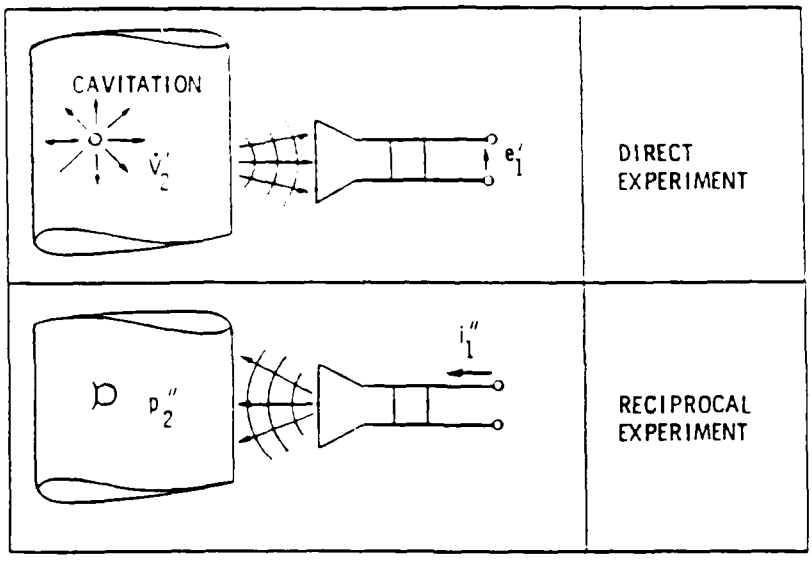

Figure 45. Determination of the Volume Velocity of a Point Source in a Water Tunnel

The volume velocity is then calculated from

$$\dot{V}' = \frac{i_1'' e_1'}{p_2''} \qquad (6.2.2)$$

At this point it has been assumed that the electro-acoustic transducers are reciprocal. One must check further to see that the entire system (which includes the water tunnel) is also reciprocal. This is accomplished by placing a projector in the tunnel and listening to it with the loudspeaker outside the tunnel. The current driving the projector is i_1' and the speaker output voltage is e_2'. Then, the direction of energy flow is reversed by driving the speaker with i_2'' and measuring the sound inside the tunnel by monitoring e_1''; the output of the projector (now a hydrophone). Transfer functions

$$\frac{i_1'}{e_2'} \quad \text{and} \quad \frac{i_2''}{e_1''}$$

are calculated and compared. If they are equal, the total system is reciprocal. Figure 46 shows these transfer functions for both the 15.3 cm and 30.5 cm water tunnels at ARL Penn State. It is clear that the direct and reciprocal experiments yield the same transfer functions, so both tunnels (and electro-acoustic transducers) are reciprocal for the frequency range shown.

Figure 47 shows a schematic view of an orifice plate mounted in the 30.5 cm water tunnel test section. Cavitation occurs in the highly turbulent mixing zone downstream of the orifice. The bubble collapse zone is where most of the noise occurs so it was

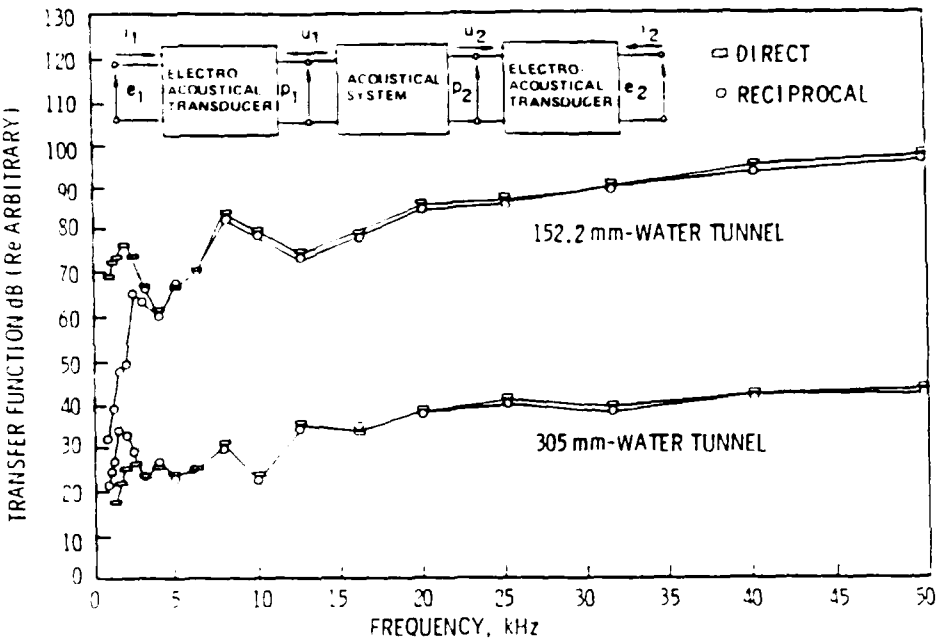

Figure 46. Direct and Reciprocal Transfer Functions for the 15.2 cm and 30.5 cm Water Tunnels at ARL Penn State

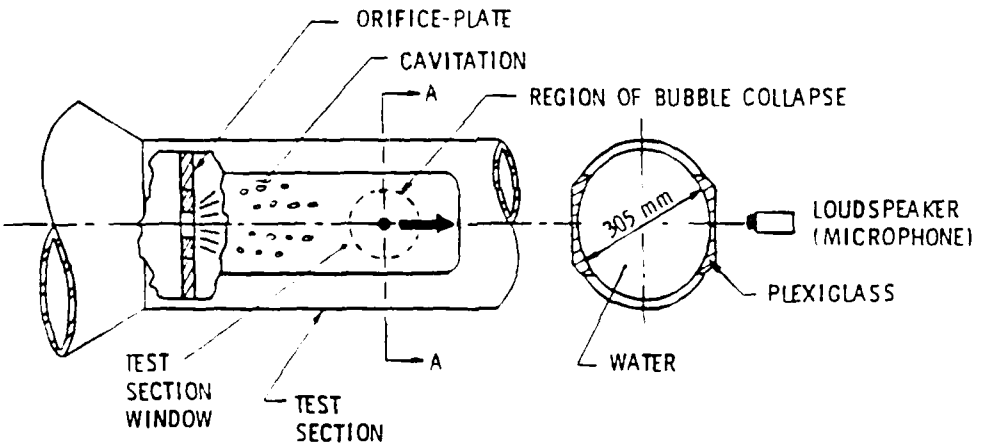

Figure 47. Schematic of Experiment on Cavitation Noise Induced by Circular Orifice Plate

there where the reciprocal transducer was placed during the calibration experiments. Figure 48 shows some typical volume velocity spectra for this type of cavitation noise. The cavitation number, K, for an orifice plate is defined by

$$K = \frac{P_d - P_v}{P_u - P_d} \qquad (6.2.3)$$

where P_d is the static pressure downstream of the plate, P_u is the upstream pressure, and P_v is the vapor pressure. The reader is referred to Bistafa (1984) for additional data and cavitation noise data scaling.

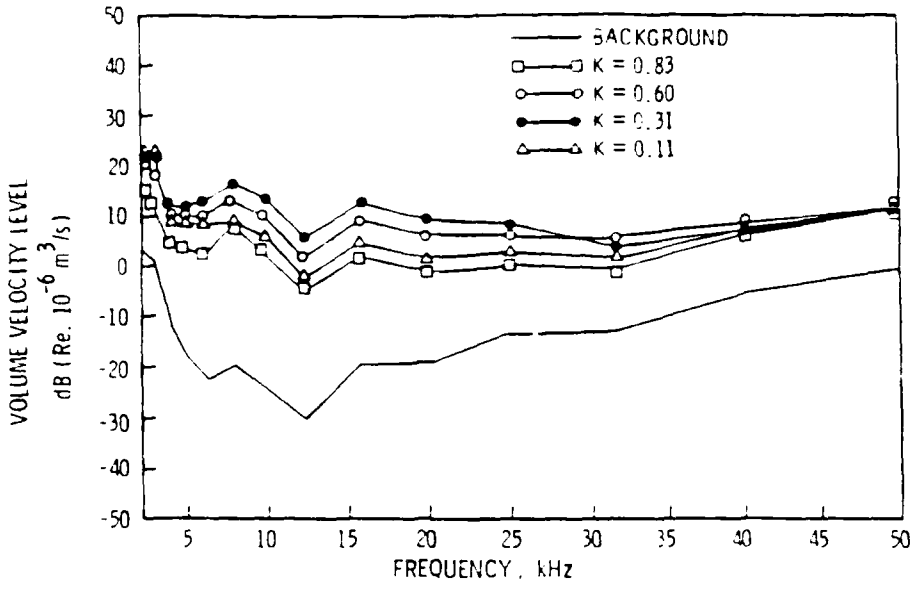

Figure 48. Typical Volume Velocity Spectra Measured Using the Reciprocity Technique for a Cavitating Orifice Plate

6.3 Background Noise Cancellation

In some instances, particularly at low frequencies, the acoustic background noise of a water tunnel can be removed from the desired noise data by a cancellation technique. The method requires that the acoustic background noise, usually caused by the pump, propagates around the tunnel circuit in plane waves. The plane wave cut-off frequency for ducts of circular cross section is accurately predicted from (Skudrzyk, 1971)

$$f_o = 0.586\ c/D\ , \qquad (6.3.1)$$

where c is the sound velocity and D is the duct inside diameter. Below this frequency, acoustic noise propagates in plane waves which are phase coherent in planes normal to the duct axis.

Suppose one is interested in measuring the wall pressure statistics under a turbulent boundary layer (TBL), say formed on the inside wall of the tunnel test section. These statistics are usually determined using flush-mounted hydrophones (in water). However, the hydrophones, when used individually, sense both the TBL noise and the tunnel background noise. If the frequency range of interest is less than f_o (given by Eq. 6.3.1) then one can use a pair of hydrophones mounted in a plane perpendicular to the test section axis. The circumferential spacing of the two hydrophones must be large in comparison to the spanwise correlation length of the TBL wall pressure fluctuations. This correlation length is typically less than the TBL displacement thickness (Willmarth, 1975), so the two pressure sensors need not be very far apart. With this arrangement, one subtracts (in real time) the two signals. The TBL contributions (the desired contributions) contained in the two signals are

statistically independent, so the subtraction does little to the statistics of the turbulence signal. However, the background noise is phase coherent and the differencing operation cancels it completely out. The difference signal thus contains only TBL information.

Lauchle and Daniels (1987) successfully used this background noise cancellation technique in the glycerine tunnel of Fig. 5. Others who have used the method include Wilson, et.al. (1979), Horne and Hansen (1981), and Simpson, et.al. (1987). It is to be noted that these latter three studies considered the cancellation of acoustic noise only, while the former study extended the technique to include vibration-induced background noise as well.

To highlight the method of Lauchle and Daniels (1987) consider Fig. 49 which shows a schematic of a co-planar three-sensor array mounted in the glycerine tunnel. Signals a(t), b(t), and c(t) are hydrophone outputs while signals $v_a(t)$ through $v_c(t)$ are accelerometer outputs. A typical hydrophone signal is decomposed; for example,

$$a(t) = a_T(t) + a_A(t) + a_V(t) + a_E(t) \qquad (6.3.2)$$

Here, one has

$a_T(t)$ - TBL wall-pressure component,

$a_A(t)$ - acoustic background noise caused by the facility,

$a_V(t)$ - vibration-induced pressure caused by the facility,

$a_E(t)$ - electronic noise component from instruments.

There are two other equations, identical to Eq. (6.3.2) for b(t) and c(t). At the outset, the electronic noise spectrum was measured with the facility off. This spectrum for a_E (or b_E, or c_E) was found to be more than 60 dB below the spectra measured with the facility on; thus, no further reference will be made to the electronic noise components.

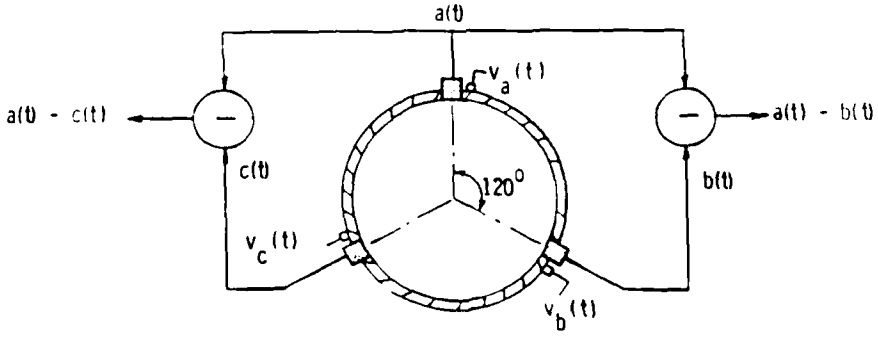

Figure 49. Schematic of a 3-Sensor Coplanar Hydrophone Array in a Tunnel Test Section

Following the spectral notation of Bendat and Piersol (1986), we see that the autospectrum of a difference signal is given by:

$$G_{a-b,a-b} = G_{a-b}$$

$$- \lim_{T_o \to \infty} (2/T_o)E[(A_T^* - B_T^* + A_V^* - B_V^* + A_A^* - B_A^*)$$

$$x\ (A_T - B_T + A_V - B_V + A_A - B_A)] \ , \qquad (6.3.3)$$

where upper-case letters denote finite Fourier transforms of the corresponding time signal, E [ ] is the expectation operation, and T_o is the record length.

Because the acoustic components (A_A and B_A) are in phase they cancel in Eq. (6.3.3). We are left with

$$G_{a-b} = \lim_{T_o \to \infty} (2/T_o)E[(A_T^* - B_T^*)(A_T - B_T)$$

$$+ (A_V^* - B_V^*)(A_V - B_V)$$

$$+ (A_V^* - B_V^*)(A_T - B_T) \qquad (6.3.4)$$

$$+ (A_T^* - B_T^*)(A_V - B_V)] \ .$$

The first product can be expanded to yield

$$\lim_{T_o \to \infty} (2/T_o)E[A_T^*A_T - A_T^*B_T - B_T^*A_T + B_T^*B_T] \ .$$

The first and fourth terms of this expansion are the autospecta of the wall-pressure fluctuations at locations a and b, respectively. Because of axisymmetry, they are equal. The middle two terms of the expansion are cross spectra of the TBL wall pressure in the spanwise (transverse) direction. These should be zero because the spacing between a and b is of order D, which is larger than the displacement thickness. Equation (6.3.4) reduces to:

$$G_T = G_{a_T} - G_{b_T}$$

$$= \frac{1}{2} G_{a-b} - \frac{1}{2} G_{a_V-b_V} - RE\ (G_{a_V-b_V, a_T-b_T}) . \qquad (6.3.5)$$

Now, if the vibration components are correlated completely over the circumference of the pipe, the second two terms of Eq. (6.3.5) will be zero and the TBL pressure spectrum is equal to one-half the auto spectrum of a difference signal.

Equation (6.3.4) is essentially described by the simple single-input, single-output model of Fig. 50. The frequency response function H(f) relates the pressure response of the transducer to normal acceleration. The broken-line path indicates

that the turbulent pressures can cause the tunnel wall to vibrate and hence contribute to the machinery-induced wall vibrations. This contribution is expected to be small because the small-area pressure transducers are dominated by the TBL energy at the convective wavenumber ($k_c = \omega/u_c$). The free-bending wavenumber of the pipe is at least an order of magnitude lower than k_c for the frequency range of measurement; thus there is not the good wavenumber matching required for there to be a strong coupling between the TBL and pipe vibration. Nevertheless, the last term of Eq. (6.3.5) describes this potential coupling.

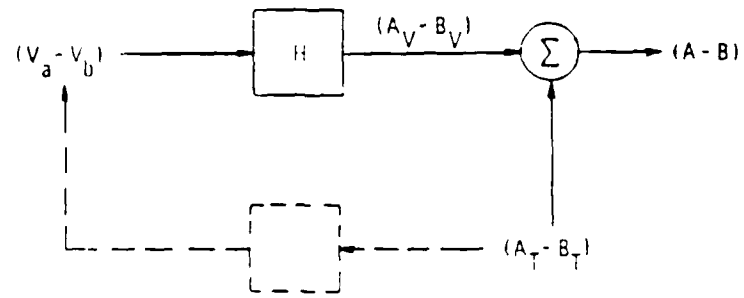

Figure 50. Schematic of a Single-Input, Single-Output Model with Extraneous Signal at the Output

In the absence of the broken-line path of Fig. 50 one can infer the relative contribution of $(V_a - V_b)$ and $(A_T - B_T)$ to (A - B) by measuring a coherent output power (COP) spectrum between the accelerometer difference signal and the pressure-transducer difference signal. That is, the COP spectrum is

$$G_{a_V-b_V} = \gamma^2_{a-b,v_a-v_b}\, G_{a-b} \tag{6.3.6}$$

and the TBL contribution is

$$G_{a_T-b_T} = (1 - \gamma^2_{a-b,v_a-v_b})\, G_{a-b} \ . \tag{6.3.7}$$

Here, the ordinary coherence function

$$\gamma^2_{xy} = |G_{xy}|^2/G_xG_y \tag{6.3.8}$$

is utilized for the measured-difference signals. Figure 51 shows typical measured spectra for G_{a-b} and the COP spectrum. Because there is a large spread between these two spectra, except at one frequency near 340 Hz, we conclude that the vibration components in the difference signal is very weak and that $(a_T - b_T)$ dominates (a-b); Eq. (6.3.5) reduces to

$$G_T = \frac{1}{2}\, G_{a-b} \ . \tag{6.3.9}$$

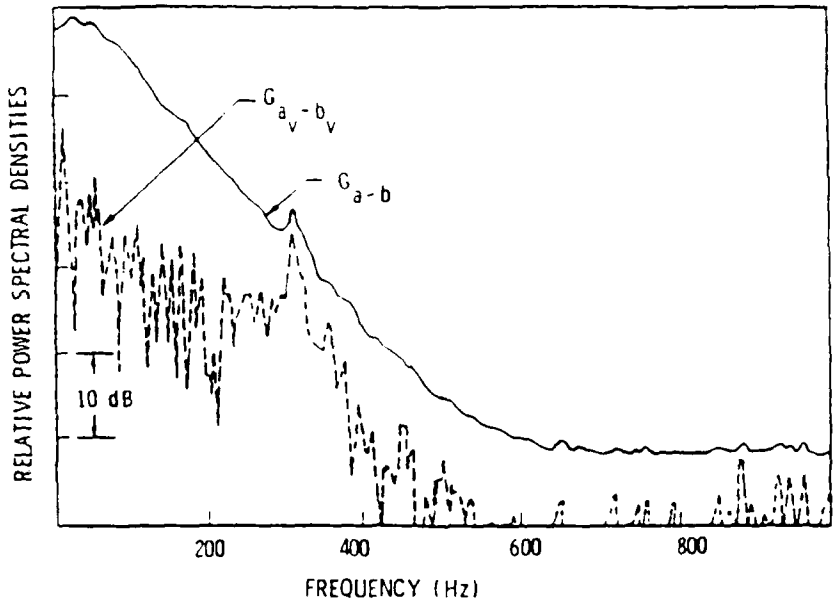

Figure 51. Spectrum of a(t)-b(t) and the Coherent Output Power Spectrum Between a(t)-b(t) and $v_a(t)$-$v_b(t)$

Figure 49 shows a third hydrophone and difference signal between it and a(t). Without showing the details (Lauchle and Daniels, 1987) it also follows that the TEL spectrum is equal to the cross spectrum between two difference signals, i.e.,

$$G_T = G_{a-b,a-c} \simeq \frac{1}{2} G_{a-b} \quad . \tag{6.3.10}$$

A verification of this is shown in Fig. 52 where it is clearly seen that $G_{a-b,a-c}$ and G_{a-b} are separated by 3 dB which is what Eq. (6.3.10) predicts.

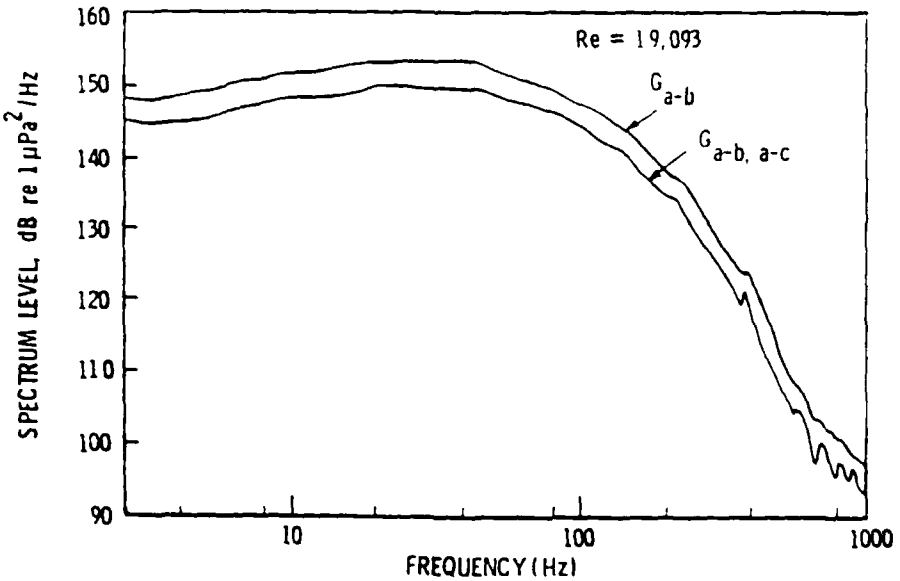

Figure 52. Spectrum of a(t)-b(t) Compared to the Cross-Spectrum Between a(t)-b(t) and a(t)-c(t)

The hydrophone differencing technique described above has enabled us to measure the TBL point spectrum in glycerine ($C_3 H_8 O_3$) pipe flow. A summary of the results are shown in Fig. 53. The spectrum level is normalized on mean flow velocity ($\bar{U}$), wall shear stress (τ_w) and inside diameter (D). The frequency is normalized on the viscous time scale (ν/u_τ^2). The importance of these data, which cover a pipe Reynolds number range of 10,000 to 26,500, lies in the value of transducer diameter (d) relative to the viscous sublayer thickness. The sublayer approaches 1 mm in this unique facility so it is a fairly easy matter of achieving values of $d^+ = u_\tau d/\nu$ of order one. It is agreed that $d^+ \approx 1.0$ for a measurement to be absent of transducer spatial averaging effects. The spectrum of Fig. 53 is not only void of transducer spatial averaging effects, but is also void of tunnel background noise.

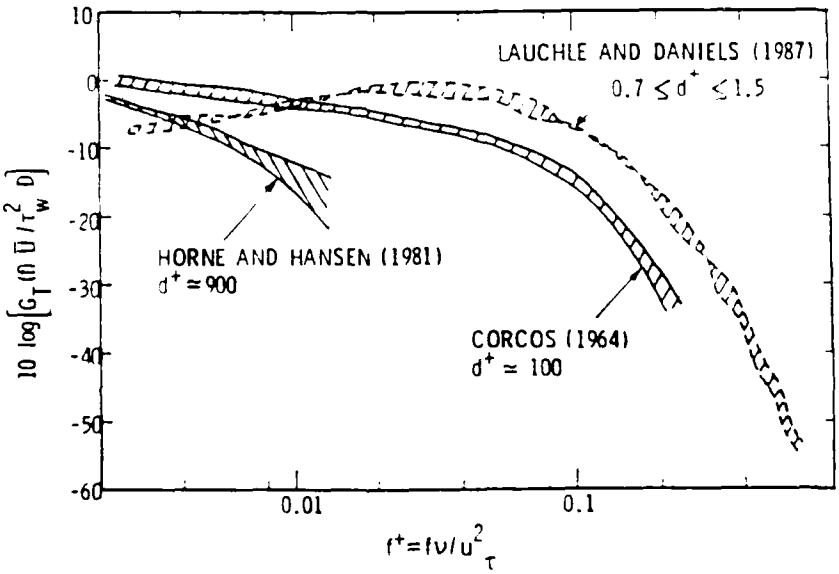

Figure 53. Normalized Wall Pressure Fluctuation Spectra Measured Under Fully-Developed Turbulent Pipe Flow (d^+=900 is in Water, d^+=100 is in Air, and d^+=1.0 is in Glycerine)

7.0 INTERNAL FLOW MEASUREMENTS

7.1 Internal Flow Measurement Facility

A High Reynolds Number Pump (HIREP) has been specifically designed to investigate high Reynolds number flow associated with internal flows of fluid handling machinery. The facility shown in Fig. 54 consists of a 1.07-m diameter pump stage driven by a 1.22-m diameter downstream turbine. The two units rotate on a common shaft and operate in the 1.22-m diameter test section of the Garfield Thomas Water Tunnel.

The facility was designed to make measurements to quantify the effects of rotor tip/end-wall clearance and rotor blade geometry on hydrodynamic loads, rotor

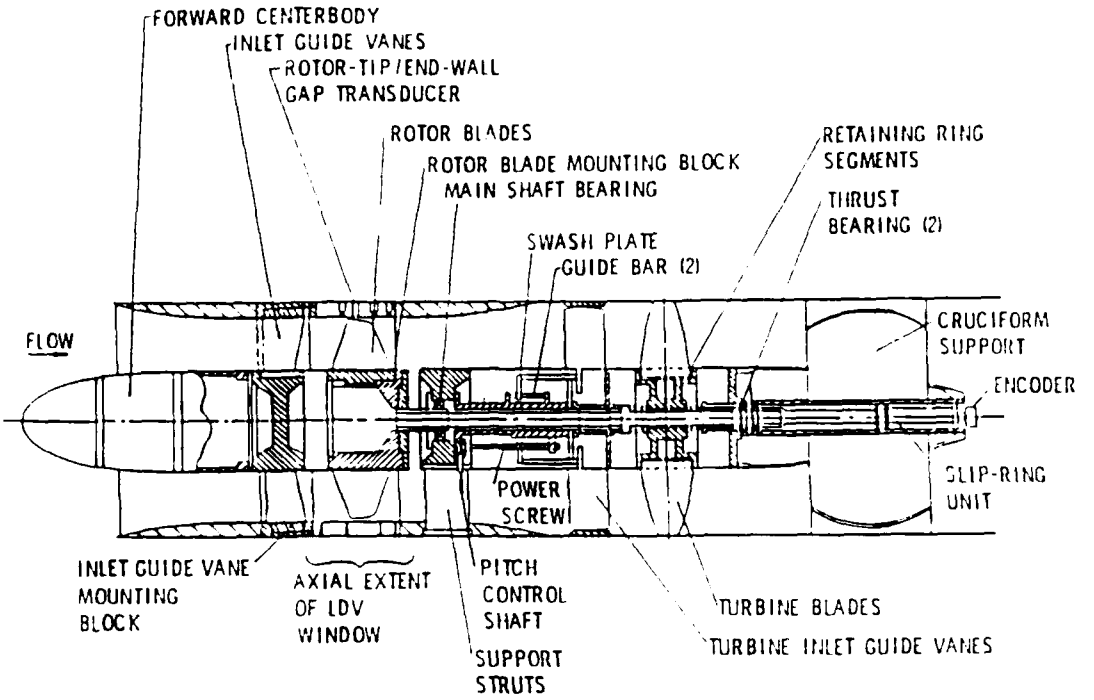

Figure 54. Schematic of HIREP Facility.

efficiency, cavitation, blade boundary layers and wakes, rotor dynamic response, and rotor-stator interactions. The flow coefficient of the pump is variable by adjusting the pitch of the turbine inlet guide vanes which are continuously variable. The operation of the pump/turbine is remarkably stable for an inlet velocity of 1.5 to 15 m/s with rotational speeds of 40-400 rpms. This range corresponds to a blade chord Reynolds number at the rotor tip of one-half million to six million.

The facility was designed to accommodate laser velocimetry measurements in the pump stage, radially traversing five-hole probes in every stage, a number of steady and unsteady pressure transducers in the rotating frame of reference, force and torque cells, and accelerometers. In addition, several advanced instrumentation systems for blade static pressure measurements, downstream stator blade unsteady pressure measurements, rotor-tip/end-wall gap measurement and cavitation viewing were developed.

A photograph of the facility installed in the test section is given in Fig. 55. Details of the hydrodynamic and mechanical design, and the operating characteristics are discussed by Farrell, McBride and Billet (1987).

7.2 Instrumentation/Measurement System

The facility contains provisions for a wide range of fluid dynamics measurements and methods. A 120-channel, low noise slip-ring unit accommodates many measurements in the rotating frame. The large, hollow chamber in the rotor hub houses an assembly of insulation displacement connectors which form the termination of the leads exiting

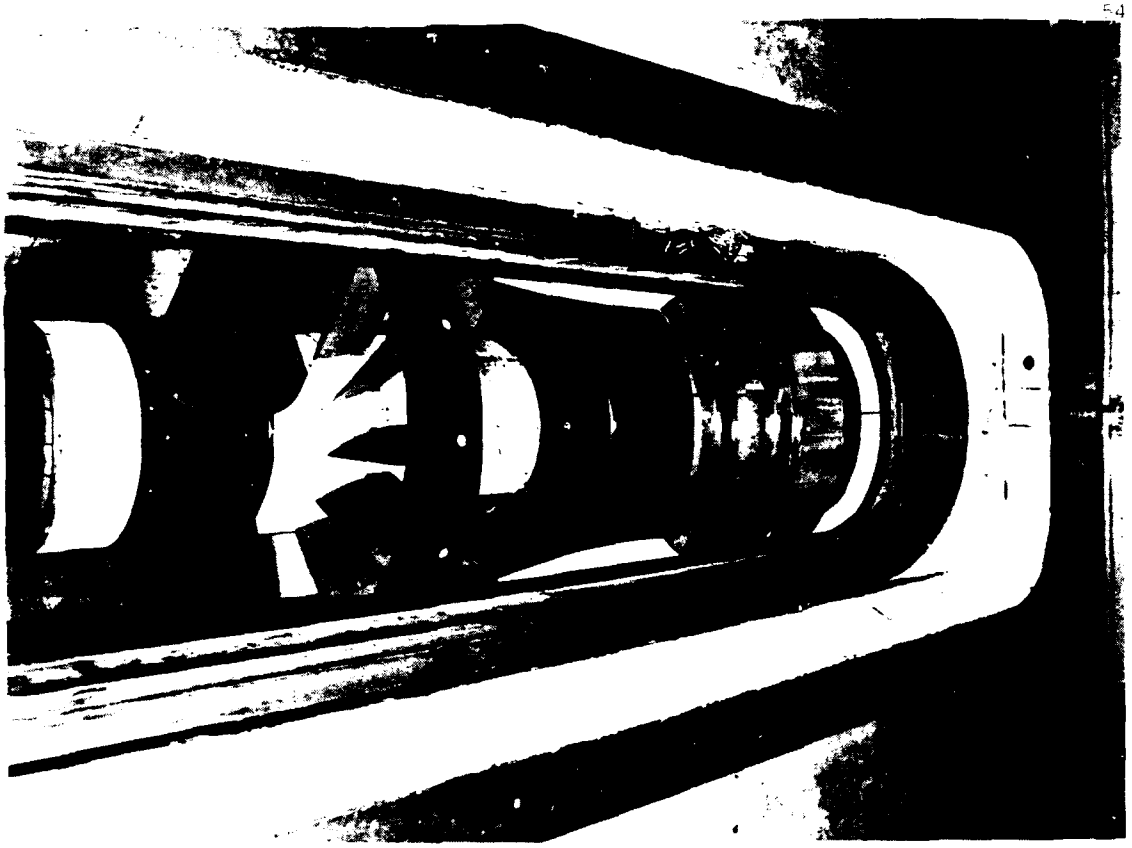

Figure 55. Photograph of HIREP Facility in the Test Section of the 1.22-m Water Tunnel.

the rotating end of the slip ring unit as shown in Fig. 56. From this termination, four ribbon cables with high flexing capability carry signals to the rotating end of

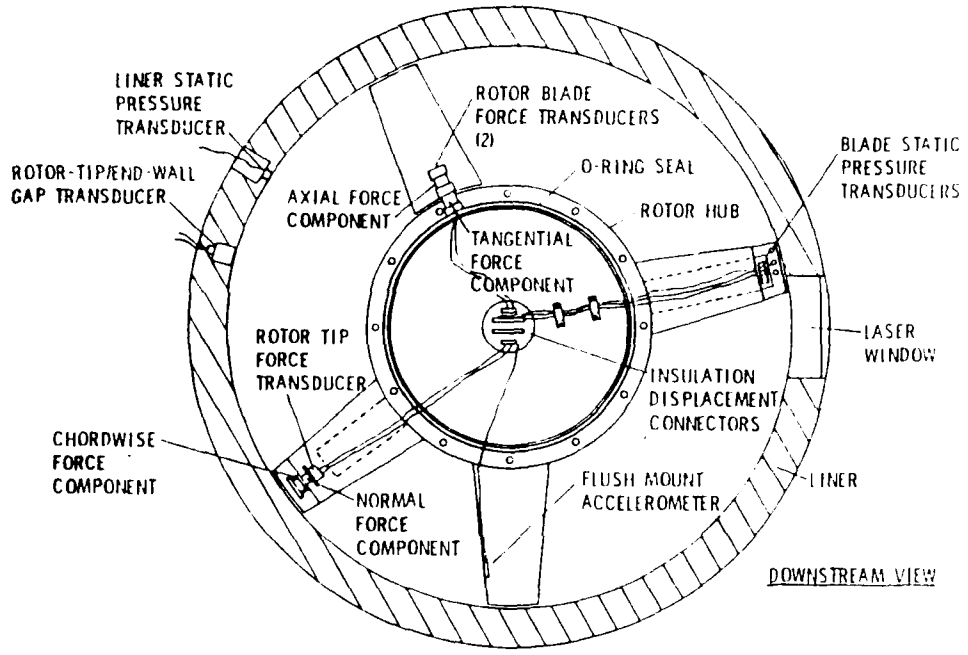

Figure 56. Rotor Hub Showing Instrumentation Capabilities.

the drive shaft. Ribbon cables form the connection between the stationary end of the slip-ring unit and the data rack and power sources outside of the facility. The signals from the transducers are sampled and processed through an extensive data analysis and reduction system consisting of the driving software program, a low pass filter, an integrating voltmeter, a multiplexer, and a VAX computer system. A schematic of the instrumentation block diagram for the performance test is shown in Fig. 57.

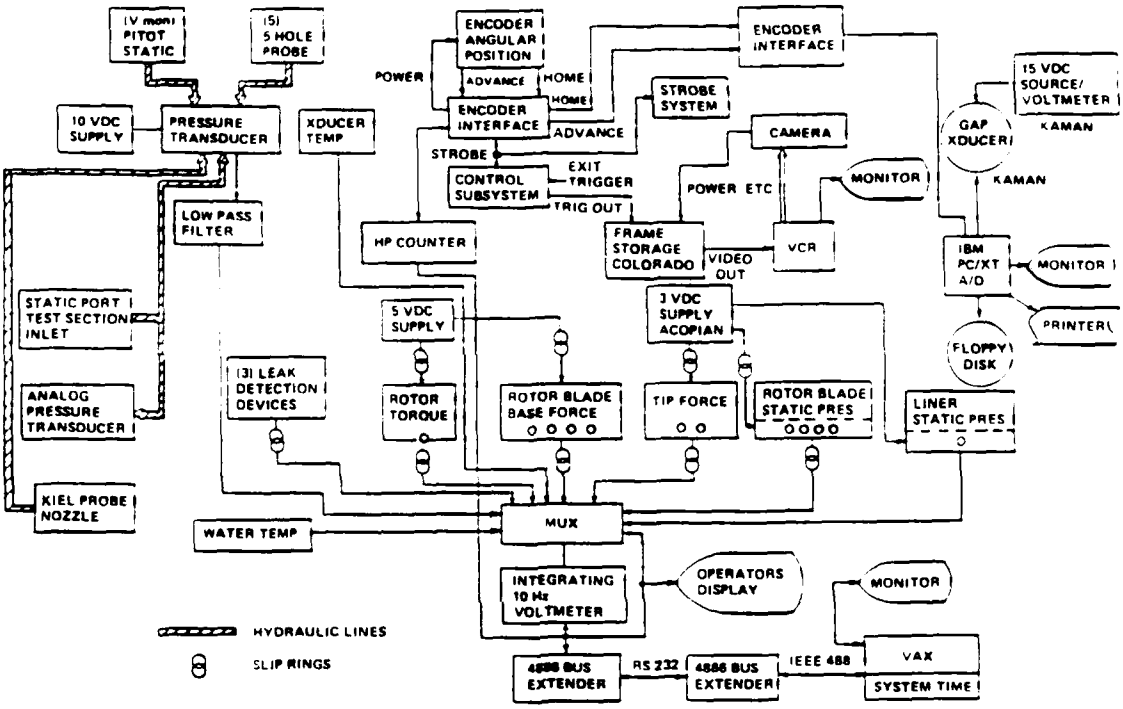

Figure 57. Instrumentation Block Diagram.

7.2.1 Velocity and Pressure Measurement

Five-hole probes can be located at the inlet and exit of the rotor, at the inlet of the turbine inlet guide vanes, and at the turbine exit. A pitot-static probe can be placed upstream of the rotor inlet guide vanes where the nose and liner are parallel and is used to calculate an axial velocity through the pump. A total pressure probe in the nozzle upstream of the test section and the static pressure port in the liner can also used to determine the axial velocity through the pump. This measurement is used as the reference axial velocity and for data normalization. The tunnel pressure control system is connected to the static pressure port. The hydraulic lines connect to a bank of differential pressure transducers located at a height equal to that of the water tunnel centerline.

The standard viewing window adjacent to the rotor is replaced by an optical window suitable for laser measurements of the rotor inlet, exit, tip-gap, and passage flows. A three-component backscatter system with a 5-watt laser is utilized for make

of these measurements. The optics/laser package is positioned by a three-axis traversing mechanism. A field point velocity measurement technique discussed by Billet (1987) is used that incorporates the instantaneous laser data with an optical shaft encoder signal. An incremental optical encoder is located on the downstream end of the shaft. In this system an angular position is associated with each instantaneous velocity measured at a point. A computer then processes this digital information.

7.2.2 Force and Torque Measurement

Forces and torque are measured on individual rotor blades and drive shaft, respectively. The rotor blade force is measured by two two-component shear beams which are mounted in the base and extend radially outward to support the lower portion of the blade span. On another blade, the outer ten percent of the blade span is instrumented with a two-component force balance to measure the normal and chordwise forces. Finally, the inner diameter of the drive shaft is strain gaged to measure torque. The excitation voltages for the strain gages are remotely sensed to correct for line loss.

7.2.3 Blade Pressure Measurement

Several pressure transducers are located in the rotor blade tip region, in the wall liner and in some cases on a downstream stator blade. For the transducers that were mounted on the rotor blade, the transducer leads are channeled through milled slots on the surface to a center hole which is drilled through the pressure and suction surfaces to a center cavity. The leads are then soldered to a small printed circuit board and ribbon cable is connected to this board. The transducers are mounted beneath a Helmholtz cavity to protect the diaphragm from high, localized pressures caused, for example, by the collapse of cavitation bubbles. During the assembly of the instrumented blade, petroleum jelly was placed into the cavity so that no trapped air would be present in the cavity.

7.2.4 Dynamic Rotor-Tip/End-Wall Measurement

A dynamic measuring system is available to measure the rotor-tip/end-wall gap. A variable impedance transducer is placed in the wall liner surrounding the rotor such that the face of the transducer is flush with the inner diameter of the liner. The impedance variation is caused by the occurrence of eddy currents in the conductive, metallic rotor tip. The coupling between the coil in the sensor and the rotor tip is dependent upon their relative displacement. Thus, the gap of any particular blade can be measured by sampling the signal from the transducer during the appropriate angular positions of the rotor as triggered by a conditioned signal from the shaft encoder. These data are processed through an A/D data acquisition system. Then software analyzes these data to determine the minimum voltage which occurs when the blade-tip

is directly over the top of the sensor face. This voltage is directly related to the gap.

7.2.5 Cavitation Inception Measurement

Cavitation inception cannot be viewed by the naked eye even with the aid of stroboscopic lighting due to the low rpm of the high Reynolds number pump. Thus, a low-rpm video viewing system is used. The low-rpm video viewing system captures a stroboscopically illuminated image and maintains a display of this image on a TV monitor until the next image has been digitized and placed in memory.

8.0 SUMMARY

A description of several important techniques used in the measurement of steady and time-dependent fluid dynamics quantities in high-Reynolds number liquid flows has been given in this Chapter. Our emphasis has been on the measurement of hydrodynamically-induced force, velocity, stress, and acoustic noise in both single and multi-phased liquid flow situations. Because water tunnels are commonly used to address high-Reynolds number liquid flows, and because they offer an extremely stable and time-invariant environment in which to conduct basic and applied fluid dynamics research, we have emphasized their use in making these measurements.

A brief introduction to the construction and operation of the typical water tunnel was given. Of particular importance is the experimenter's ability to maintain constant values of free-stream velocity and ambient pressure. Also, with appropriate sub-systems, the water (or other liquid) temperature and quality (free and dissolved gas content and particulate matter) can be controlled. Temperature control is particularly important if one wishes to raise (or lower) the unit Reynolds number range of the facility. Turbulence in the test section can also be controlled by placing the appropriate screens and honeycomb far upstream in the tunnel settling section. It was pointed out that the control of acoustic background noise in water tunnels is quite difficult, but that the elimination of all sources of facility-generated cavitation is the first most important step to effective noise control.

Body force and moment measurements are routinely conducted at high Reynolds numbers in water tunnels and towing tanks. The sensors used in such tests are usually strain-gaged balance devices. We emphasized that when large bodies (relative to the test section diameter) are tested, spurious forces and moments can be created by blockage effects and by horizontal buoyancy (viscous) effects. Methods to account for these problems were discussed.

There are many problems associated with making detailed measurements in laminar and turbulent liquid boundary layers at high speed. One of the more serious of these problems is the very small size of the inner scales of the turbulent boundary layers. Optical techniques, such as Laser Doppler Velocimetry (LDV), or techniques which employ surface measurement devices, such as flush-mounted hot film probes have proven most effective. Often, however, the spatial scales of the measurement devices

are so large that significant averaging of the results is unavoidable. In addition, the very near-wall regions of a turbulent boundary layer are often not accessible to measurement. Thus, while water tunnels are the proper choice for the study of phenomena associated mainly with high Reynolds number liquid flows, such as many drag reduction mechanisms, they are generally not the proper choice for fundamental studies of the turbulent boundary layer.

Measurements in multiphased flows are difficult to generalize since each given flow situation usually requires a unique measurement technique. One of the most widely used techniques, however, is some form of flow visualization. This includes the use of tufts, oil paint films, injected dyes, bubble tracking, Schlieren photography, light scattering techniques, and holographic photography. The use of some of these methods in cavitation research was discussed with emphasis on the measurement of bubble distributions using scattered laser light, and on the measurement of cavitation bubble dynamics using holography.

Flow-induced acoustic noise can be measured in some water tunnels using reverberation room acoustic measurement techniques or special techniques developed for the specific tunnel and tunnel test. The methods usually involve the use of single hydrophones or arrays of hydrophones. Hydrophone directivity is important because it can be used to improve the signal-to-noise ratio; the more directive is the receiver, the more it can be used to discriminate the desired source of noise from the background sources of noise. We presented a discussion on the calibration and use of a reflector-type hydrophone in radiated noise measurements. A non-intrusive method of making acoustic measurements in a water tunnel (or any other closed flow facility) based on the theory of acoustic reciprocity was also presented. The method is quite new and provides the hydroacoustics experimenter a method whereby the source strength of an acoustic source can be measured directly. Wall pressure fluctuations under turbulent boundary layers is a subject of importance, but many measurements are inaccurate because of transducer spatial averaging problems, facility background noise (particularly at low frequencies), and the paramount difficulties of implementing wide area transducer arrays for mapping the space/time statistics of these pressure fluctuations. The issues of background noise and transducer resolution were described in detail with a specific measurement example given to verify that both problems can be eliminated. This example used a passive background noise cancellation technique together with sub-miniature pressure transducers under a glycerine turbulent boundary layer.

The measurement of cavitation inception, cavitation noise, local pressure and velocity fields, and body (surface) forces and moments within complex liquid handling turbomachines under realistic high-Reynolds number operation is an extremely difficult undertaking. In this Chapter we have described one way of approaching this important problem. The method virtually models an axial-flow turbomachine outer casing by a water tunnel test section. The viewing windows in the test section permit almost total visual access to the internal hydrodynamics of the turbomachine; thus, flow

visualization, conventional LDV, and specialized internal probing can be achieved. The Reynolds number range of such experiments can be very large if large tunnels coupled with high-speed operation are used.

REFERENCES

Alfredsson, P. H., Johansson, A. V., Haritonidis, J. H. & Eckelmann, H. 1988 The fluctuating wall-shear stress and velocity field in the viscous sublayer. Phys. Fluids 31, 1026-1033.

Bajura, R. A. & Billet, M. L., ed. 1986 Fluid Measurements and Instrumentation Forum - 1986, ASME, (Atlanta, Georgia).

Bakewell, H. P. & Lumley, J. L. 1967 Viscous sublayer and adjacent wall region in turbulent pipe flow. Phys. Fluids 10, 1880-1889.

Bakewell, H. P. 1968 Turbulent wall-pressure fluctuations on a body of revolution. J. Acoust. Soc. Am. 43, 1358-1363.

Barker, S. J. 1974 Measurements of radiated noise in the CALTECH high-speed water tunnel. Graduate Aeronautical Lab Report NR 062-462.

Barker, S. J. & Gile, D. 1981 Experiments on heat stabilized laminar boundary layers in water. J. Fluid Mech. 104, 139-158.

Barker, S. J. 1973 Radiated noise from turbulent boundary layers in dilute polymer solutions. Phys. Fluids 16, 1387-1394.

Bellhouse, B. J. & Schultz, D. L. 1966 Determination of mean and dynamic skin friction, separation and transition in low speed flow with a thin film heated element. J. of Fluid Mech. 24, 379.

Bendat, J. S. & Piersol, A. D. 1986 Random Data, 2nd Ed. (Wiley, New York) p. 132.

Besant, W. 1859 Hydrostatics and Hydrodynamics, Cambridge University Press, Cambridge, England.

Billet, M. L. 1987 Wake measurments using a laser doppler velocimeter system. Proceedings of The International Towing Tank Conference, Kobe, Japan.

Billet, M. L. 1986 Cavitation nuclei measurments with an optical system. J. of Fluids Engr., 108, 366-372.

Bistafa, S. R. 1984 An experimental study on the noise generated by vaporous cavitation in turbulent shear flows produced by confined orifice plates. Ph.D. Thesis, The Pennsylvania State University.

Bistafa, S. R., Lauchle, G. C. & Reethof, G. 1987 Noise generated by cavitation in orifice plates. To appear in J. of Fluids Engr.

Blake, W. K. 1986 Mechanics of Flow-Induced Sound and Vibration, Vol. I and II (Academic Press, Orlando).

Blake, W. K., Wolpert, M. J. & Geib, F. E. 1977 Cavitation noise and inception as influenced by boundary-layer development on a hydrofoil. J. Fluid Mech. 80, 617-640.

Chahine, G. & Shen, Y. T. 1985 Bubble dynamics and cavitation inception in cavitation susceptability meters. Proc. Int. Sym. on Fundamental Aspects of Gas-Liquid Flows (Miami Beach, Florida).

Coles, D. E. 1968 A young person's guide to the data. In Proceedings of the AFOSR-IFP Stanford Conference on Computation of the Turbulent Boundary Layers, D. E. Coles and E. A. Hirst, Eds., Stanford University Press, Stanford, CA.

Corcos, G. M. 1964 The structure of the turbulent pressure field in boundary layer flows. J. Fluid Mech. 18, 353.

D'Agostino, L. & Acosta, A. J. 1983 On the design of cavitation susceptability meters (U.S.M.'s). Proc. 24th American Towing Tank Conference (Hoboken, New York).

Deutsch, S. & Castano, J. 1986 Microbubble skin friction reduction on an axisymmetric body. Phys. of Fluids 29, 3590.

Dybbs, A. & Pfund, P. A. 1985 International Symposium of Laser Anemometry, ASME, Miami Beach, Florida).

Eckelmann, H. 1974 The structure of the viscous sublayer and adjacent wall region in a turbulent channel flow. J. Fluid Mech., 65, 439.

Farmer, W. M. 1976 Sample space for particle size and velocity measuring interferometers. Applied Optics, 15, No. 8.

Furuya, O. 1987 Cavitation and Multiphase Flow Forum - 1987, ASME (Cincinnati, Ohio).

Farrell, J. J., McBride M. W. & Billet, M. L. 1987: High Reynolds number pump facility for cavitation research. Proc. Int. Sym. on Cavitation Research Facilities and Techniques - 1987 (Boston, Massachusetts).

Gates, E. M. & Bacon, J. 1978 Determination of cavitation nuclei distributions by holography. J. Ship Res., 22, 29-31.

Gad-el-Hak, M. 1987 The water towing tank as an experimental facility, an overview. Exp. in Fluids 5, 289-297.

Gavigan, J. J., Watson, E. E. & King, W. F. 1974 Noise generation by gas jets in a turbulent wake. J. Acoust. Soc. Am. 56, 1094-1099.

Gowing, S. & Ling, S. C. 1980 Measurements of microbubbles in a water tunnel. Proc. 12th American Towing Tank Conference (Ann Arbor, Michigan).

Greshilov, E. M. & Mironov, M. A. 1983 Experimental evaluation of sound generated by turbulent flow in a hydrodynamic duct. Sov. Phys. Acoust 29, 275-280.

Hall, W. R. 1973 Tunnel wall interference for bodies-of-revolution in non-steady motion. Master of Science Thesis, The Pennsylvania State University.

Hamilton, M. F., Thompson, D. E. & Billet, M. L. 1986 An experimental study of travelling-bubble cavitation noise. J. of Fluids Engr. 108, 241-247.

Hammitt, F. G., Keller, A., Ahmed, O., Pyun, J. J. & Tilmaz, E. 1974 Observation and measurement of cavitation nuclei using Coulter counter and laser light scattering in cavitation and multiphase flow laboratory at the University of Michigan. Report No. VMICH 03157-24-I.

Hanratty, T. J. & Campbell, J. A. 1982 Measurement of wall shear stress. In Fluid Mechanics Measurements, (R. J. Goldstein, Ed.), Hemisphere Publishing Corporation, New York.

Henderson, R. E. & Parkin, B. R. 1982 Hydrodynamic test facilities at ARL Penn State. Proc. 2nd Defense Research Group Seminar on Adv. Hydro. Test Facilities. NATO DS/A/DR 83052.

Holl, J. W. 1970 Nuclei and cavitation. J. of Basic Engr. 92, 681-688.

Holl, J. W., Billet, M. L. & Weir, D. 1975 Thermodynamic effects on developed cavitation. J. of Fluids Engr. 97, 507-514.

Holl, J. W. & Billet, M. L. 1987 International Symposium on Cavitation Research Facilities and Techniques - 1987 ASME, Boston, Massachusetts, December 1987.

Horne, M. P. & Hansen, R. J. 1981 Minimization of farfield acoustic effects in turbulent boundary layer wall pressure fluctuation experiments. Proc. 7th Symp. on Turb. (Univ. Missouri, Rolla) p. 139.

Hadvkov, I. F. & Lvamshev, L. M. 1970 Influence of polymer additives on the pressure fluctuations in a boundary layer. Sov. Phys. Acoust. 16, 59-63.

Keller, A. P. 1972 The influence of the cavitation nucleus spectrum on cavitation inception, investigated with a scattered light counting method. J. of Basic Engr., 94, 917-925.

Kohler, R. A. & Billet, M. L. 1981 Light scattering by a nonspherical particle. Cavitation and Polyphase Flow Forum - 1981 (Boulder, Colorado).

Ladd, D. M. & Hendricks, E. W. 1985 The effects of background particulates on the delayed transition of a heated 9:1 ellipsoid. Exp. in Fluids 3, 113-119.

Lauchle, G. C. 1977 Noise generated by axisymmetric turbulent boundary-layer flow. J. Acoust. Soc. Am. 61, 694-703.

Lauchle, G. C. 1979 Horizontal buoyancy effects on the pressure distribution of a body in a duct. J. Hydronautics 13, 61-67.

Lauchle, G. C. 1983 In-duct viscous flow pressure distribution on a body with boundary-layer control. J. Ship Res. 27, 34-38.

Lauchle, G. C., Eisenhuth, J. J. & Gurney, G. B. 1980 Boundary-layer transition on a body of revolution. J. Hydronautics 14, 117-121.

Lauchle, G. C. & Gurney, G. B. 1984 Laminar boundary-layer tranistion on a heated underwater body. J. Fluid Mech. 144, 79-101.

Lauchle, G. C. 1974 Dynamic hinge moment of a low aspect ratio control surface. J. Hydronautics 8, 119-120.

Lauchle, G. C. & Daniels, M. A. 1987 Wall-pressure fluctuations in turbulent pipe flow. Phys. of Fluids 30, 3019-3024.

Lecoffre, Y. & Bonnin, J. 1979 Cavitation tests and nucleation control. Proc. Int. Sym. Cavitation Inception (New York, New York).

Lehman, A. F. 1959 The Garfield Thomas Water Tunnel. Ordnance Research Laboratory, The Pennsylvania State University Tech. Report NOrd 16597-56.

Lehman, A. F., Light, J. H. & Peirce, T. E. 1958 Elimination of water-tunnel interaction with a coaxial test body by a flow correcting liner. Ordnance Research Laboratory, The Pennsylvania State University, Report NOrd 16597-59.

Liepmann, H. & Skinner, J. 1954 Shearing-stress measurements by use of a heated element. NACA TN 1924

Ludwieg, H. 1950 Instrument for measuring the wall shearing stress of turbulent boundary layers. NACA TM 1284.

Ludwieg, H. & Tillmann, W. 1950 Investigation of the wall shearing stress in turbulent boundary layers. NACA TM 1285.

Lumley, J. L. 1964 Passage of a turbulent stream through honeycomb of large length-to-diameter ratio. Trans. A.S.M.E., J. Basic Engr. 886, 218-220.

Lumley, J. L. & McMahon, J. F. 1967 Reducing water tunnel turbulence by means of a honeycomb. Trans. A.S.M.E., J. Basic Engr. 89, 764-770.

Lyamshev, L. M., Chelnokov, B. I. & Shustikov, A. G. 1984 Pressure fluctuations in a turbulent boundary layer under the conditions of injection of a continous medium through a permiable boundary. Sov. Phys. Acoust. 30, 394-397.

Maidanik, G. & Jorgensen, D. W. 1967 Boundary wavevector filters for the study of the pressure field in a turbulent boundary layer. J. Acoust. Soc. Am. 42, 494-501.

Marboe, R. C. 1982 Bubble dynamics and resulting noise from traveling bubble cavitation. M.S. Thesis, Massachusetts Inst. Tech. Also, ARL TM No. 82-94, The Pennsylvania State University).

Medwin, H. 1977 Acoustical determination of bubble size spectra. J. of Acoust. Soc. Am. 62, 1041-1044.

Oba, R. 1981 Cavitation nuclei measurments by a newly made Coulter counter without adding salt in water. Rep Inst. High Speed Mech. (Tohoku University) 43, 340.

Oldenziel, D. M. 1979 New instrument in cavitation research. Proc. Int. Sym. Cavitation Inception (New York, New York) 111-124.

Oosterveld, M. W. C. & Johnson, B. 1985 16th International Towing Tank Conference Catalog of Facilities (Contact Prof. Bruce Johnson, U.S. Naval Academy, Annapolis, MD 21402, U.S.A.).

Parkin, B. R. 1983 Hydrodynamics and fluid mechanics. Naval Research Rev. 35, 20-34.

Peirce, T. E. 1964 Tunnel wall interference effects on drag and pitching moment of an axisymmetric body. Ph.D. Thesis, The Pennsylvania State University.

Ramjee, V. & Hussain, A.K.M.F. 1976 Influence of the axisymmetric contraction ratio on free-stream turbulence. Trans. A.S.M.E., J. Basic Engr. 98, 506-515.

Robbins, B. E. 1978 Water tunnel turbulence measurements behind a honeycomb. J. Hydronautics 12, 122-128.

Ross, D., Robertson, J. M. & Power, R. B. 1948 Hydrodynamic design of the 48-inch water tunnel at the Pennsylvania State University. S.N.A.M.E. Trans. 56, 5-29.

Sandborn, V. A. 1979 Surface shear stress fluctuations in turbulent boundary layers. In Proceedings of the Second Symposium on Turbulent Shear Flow, Imperial College, London.

Schiebe, F. R. & Killen, J. M. 1971 An evaluation of acoustical techniques for measuring gas bubble size distributions in cavitation research. St. Anthony Falls Hydraulic Lab No. 120. University of Minnesota).

Schloemer, H. H. 1974 Installation of a rectangular test section for acoustic water tunnel studies of flow-induced noise. NUSC Tech. Report 4763.

Sevik, M. 1964 Measurement of unsteady thrust in turbo-machinery. A.S.M.E. Paper 64-FE-15.

Shen, Y. T.; Gowing, S. 1985 Scale effects on bubble growth and cavitation inception in cavitation susceptability meters. Cavitation and Multiphase Flow Forum - 1985 (Albuquerque, New Mexico) 14-16.

Simpson, R. L., Ghodbane, M. & McGrath, B. E. 1987 Surface pressure fluctuations in a separating turbulent boundary layer. J. Fluid Mech. 177, 167-186.

Skudrzyk, E. J. & Haddle, G. P. 1960 Noise radiation from a turbulent boundary layer by smooth and rough surfaces. J. Acoust. Soc. Am. 32, 19-34.

Skudrzyk, E. 1971 The Foundations of Acoustics, Basic Mathematics and Basic Acoustics (Springer, New York) p. 330.

Tam, C. K. W. 1975 Intensity, spectrum, and directivity of turbulent boundary layer noise. J. Acoust. Soc. Am. 57, 25-34.

Thompson, D. E. 1976 Propeller time-dependent forces due to non-uniform inflow. Ph.D. Thesis. The Pennsylvania State University.

Vikram, C. S. & Billet, M. L. 1983 Gaussian beam effects in far-field in-line holography. Applied Optics. 22, 2830-2835.

Vikram, C. S. & Billet, M. L. 1984 Optimizing image-to-background irradiance in far-field in-line holography. Applied Optics 25, 1995-1998.

Vikram, C. S. & Billet, M. L. 1984 In-line Fraunhofer holography of a few far fields. Applied Optics 23. 3091-3094

Vikram, C. S. & Billet, M. L. 1982 Holographic image formation of objects inside a chamber. Optik 61, No. 4, 427-432.

Vikram, C. S. & Billet, M. L. 1983 Magnification with divergent beams in Fraunhofer holography of object inside a chamber. Optik 63, No. 2, 109-114.

Waterhouse, R. V. 1958 Output of a sound source in a reverberation chamber and other reflecting environments. J. Acoust. Soc. Am. 30, 4-13.

White, F. M. 1974 Viscous Fluid Flow, (McGraw-Hill, New York).

Willmarth, W. W. 1975 Pressure fluctuations beneath turbulent boundary layers. Ann. Rev. Fluid Mech. 7, 13-37.

Wilson, R. J., Jones, B. G. & Roy, R. P. 1979 Measurement technique of stochastic pressure fluctuations in annular flow. Proc. 6th Symp. on Turb. (University Missouri, Rolla), p. 4-1.

Wolde, T. T. 1973 Reciprocity experiments on the transmission of sounds in ships. Ph.D. Thesis, Delft University, The Netherlands.

Yungkurth, C. B. 1983 A light-scattering system to measure cavitation nuclei analysis and calibration. M.S. Thesis. The Pennsylvania State University.